The Effect of the Mixture Composition of $BmimBF_4$-Acetonitrile on the Excited State Relaxation Dynamics of a Solar Cell Dye D149: An Ultrafast Transient Absorption Study

Nishith Maity,[a] Piotr Piatkowski,[b*] Kamil Polok,[b*] François-Alexandre Miannay,[a] Abdenacer Idrissi[a*]

[a] Universiy of Lille, CNRS, UMR 8516-LASIRe, Laboratoire Avancé de Spectroscopie pour les Interactions, la réactivité et l'Environement, F-59000 Lille, France

[b] Faculty of Chemistry, Laboratory of Spectroscopy and Intermolecular Interactions, University of Warsaw, Żwirki i Wigury 101, Warsaw 02-089, Poland

e-mail:- Nacer.Idrissi@univ-lille1.fr

ABSTRACT

The excited state relaxation dynamics of D149, one of the metal free substituted indoline dyes used in dye sensitized solar cells, is studied in whole composition range of $BmimBF_4$-acetonitrile binary mixture by using time-integrated absorption, emission and time-resolved transient absorption (TA) spectroscopies. The comparative analysis of absorption and emission spectra indicate that the value of Stokes shift reduces monotonically with decreasing mixture polarity. The global analysis of time-resolved TA spectra indicates the presence of four different time components related to different processes in the excited state of the dye. Importantly, the observed timescales are highly sensitive to composition, polarity and viscosity of the binary mixture. Increase of viscosity and decrease of polarity observed for increasing ionic liquid content in the mixture, lead to overall increase in the emission lifetime (S_1-S_0) of D149. At lower ionic liquid mole fraction (X_{IL} = 0.1), the emission lifetime, shows a minimum that can be traced back to the change from the situation where the local environment of the dye is dominated by the interactions in acetonitrile to that where it is dominated by those in $BmimBF_4$. This also is reflected in the occurrence of a minimum in relative quantum yield in the same range of X_{IL}. The origin of the other moderately long-time component (33 ps in ACN-120 ps in $BmimBF_4$) is still debatable; however, for pure ionic liquid and all the mixtures, the composition dependence of this timescale is similar to that of the longest emission lifetime.

1. INTRODUCTION

After the invention of Dye Sensitized Solar Cell (DSSC) by Grätzel and O'Regan in 1991,[1] scientists got new areas of interest related to optimization of the efficiency of this type of solar cell. DSSC is a 3rd generation photovoltaic device whose power conversion efficiency (PCE) exceeds 14%.[2–4] The overall efficiency of DSSC depends on three factors which are light absorption efficiency of the dye, charge injection efficiency of photoexcited charge carriers and

charge collection efficiency in the electrodes.[5] Thus, the two key components for DSSC overall efficiency are the electrolyte and the sensitizer (dye). There are number of theoretical and experimental publications dedicated to optimizing the cell efficiency of DSSC by varying these two components.[6–10]

Nowadays, ionic liquids (ILs) are considered as an electrolyte due to some of their interesting properties over traditional solvents like stability, high conductivity, large electric potential window.[11,12] Despite all these advantages of ILs, their high viscosity and high cost limit their use in DSSC. A trade-off between the desired and undesired properties is obtained when IL is mixed with a molecular solvent at a specific mole fraction.[13] In this way, both the electrolyte viscosity and the cost of DSSC can be decreased.

The values of densities, viscosities[14,15] and conductivities[16] of different ionic liquid-molecular solvent (IL-MS) binary mixtures are well-documented. For instance, Stoppa et al. showed an initial increase of ionic conductivity in several ionic liquid-polar solvent mixtures due to the increase in the number of ions; however, after reaching the maximum at $X_{IL} \approx 0.1$-0.25 (varies between binary mixtures), the conductivity value starts to decrease due to increase in viscosity (and consequently, decrease of ion mobility) of the mixtures. According to Buchner et al., IL-MS mixtures behave like lubricated ionic liquid down to $X_{IL} \approx 0.2$. Below that concentration, their properties are similar to the conventional electrolyte solutions. In the transition region at $X_{IL} \approx 0.2$, the redissociation of the ion pairs of IL occurs that eventually helps to build an IL-like structures.[17] However, the notion of polarity of these IL-MS mixtures, that is important when studying the photophysics of a dye, is quite contradictory. Indeed, the solvatochromic polarities of ILs are quite high (same range as short chain alcohols), while their statistic dielectric constants are quite low (same range as medium chain-length alcohols like n-pentanol).[18] Due to the presence of ions in the IL-MS mixture, the concept of polarity is not similar to the one which we are used to in the case of conventional solvents.[18,19]

Another important component of DSSC is the photosensitizer (dye) and its optimization has been addressed in several papers.[20–26] Traditional dyes with metal center can be replaced by the metal free organic ones, namely D205, D149, D102, D131 etc., with common substituted indoline donor moiety D.[27] These are more environment friendly and less expensive compared to the dyes with metal centers.[25] These type of organic dyes were designed to have a donor-anchor group-acceptor (D-π-A) structure. Therefore, the charge transfer occurs from the donor unit to the acceptor unit and the electron injection to the electron transporting layer (ETL) occurs through the electron withdrawing anchor group (like -COOH, $-SO_3H$ group).[25]

The overall efficiency of DSSC primarily results from effective light absorption by photosensitizer followed by the injection of photoexcited charge carriers to the ETL. The reasons behind the decrease in the efficiency of DSSC are the occurrence of reverse processes: back charge transfer to sensitizer and direct recombination between electron and hole transporting layers. Several reports show a scheme of different dynamical processes within a typical DSSC.[5,28,29] According to these, all the forward reactions that are helpful for the higher efficiency of DSSC are quite fast as compared to the unfavorable electron recombination from semiconductor conduction band to the sensitizer or to the redox pair. Hence, these are not very disadvantageous to DSSC; however, sometimes the lifetime of the sensitizer molecule in the excited state (depending upon the type of sensitizers used in DSSC) is comparable to the forward reactions rate in DSSC and can cause decrease in the efficiency of the solar cell.[25]

Therefore, studies of the excited state dynamics in the sensitizers are necessary for further development of DSSC.

Some recent reports have also dealt with the excited state dynamics of the indoline-based dyes, that are a promising class of photosensitizers, dissolved in various neat solvents differing by their ability to form hydrogen bond, polarity and viscosity.[30–35] For instance, Fakis et al. used femtosecond up-conversion spectroscopy to study the dynamics of D149 in different organic solvents and PMMA films.[32] Then Lohse et al. used femtosecond pump-supercontinuum probe (PSCP) spectroscopy and time correlated single photon counting (TCSPC) to get an idea about D149 photophysics in different organic solvents.[30] El-Zohry et al. published a series of papers on the excited state in the D149 dye. All of these reports together give idea about different excited state processes in the D149 dye like photoisomerization and aggregation,[33] excited state proton transfer (ESPT)[35] and ultrafast twisting around vinyl double bond in D149 donor moiety.[34] Additionally, Lin et al. also showed that isomerization process of the sensitizer affects the efficiency of the cell.[31] All these competitive processes result in decrease in the efficiency of the solar cell. The authors also suggested these competitive processes could be countered by attaching the dye to a semiconductor oxide electrode[33] and introducing quasi solid[32] and solid[33] states as the medium surrounding the dye molecules.

These investigations show that the D149 relaxation dynamics consists of four different timescales of which two faster ones are related to solvation dynamics.[30,32,34] Furthermore, the relaxation of excited state of the dye (D149) contains two more timescales which are quite longer than the solvation dynamics timescales. The faster one was attributed previously to vibrational relaxation/structural relaxation of the dye excited state.[30,32] However, El-Zohry et al. showed that this fast relaxation timescale is due to a twisting motion around the double bond in the donor unit of the dye.[34] The other, slow relaxation time was previously attributed to S_1-S_0 decay of the dye molecule.[30,32,34] This slow component also depends on the polarity of the medium surrounding the dye.[30,32]

Surprisingly, we are not aware of any investigation of the photophysics of the D149 in IL or in IL-MS mixture. However, there are many studies where Coumarin 153 (C153) was used as model dye to rationalize its solvation dynamics in ILs. [36–41] For instance, in a mixture of C153 with ILs there is a convergence to interpret the sub-picosecond relaxation time as related to the inertial motions of the solvent and ions and the slower one as related to the structural reorganization of the ions surrounding the solute (dye) molecule.[36–41] It was also found that the solvation dynamics in IL is slower as compared to that in common solvents such as acetonitrile, methanol, and water. In particular, the solvation dynamics of C153 in $BmimBF_4$ showed that the overall solvation process has two time constants of 278 ps and 3.98 ns.[42] The work of Maroncelli et al. showed that solvation times of C153 display an approximate power law relationship with viscosity of solvent mixture of $BmimBF_4$ and acetonitrile.[41,43] According to a review by Samanta, solvation processes in ionic liquids are not similar to those in organic solvents. The dipole-dipole interactions are dominant in the case of pure organic solvents, while in ionic liquids the interactions between charged groups of the ions and polar molecules of solute play the major role in the solvation process. The orientational relaxation of free ions also plays an important role in solvation dynamics of those compounds.[36]

Furthermore, there are very few studies on the excited state dynamics of dyes (other than D149) in IL-MS binary mixtures.[44–48] Due to the presence of ions in ionic liquids,

molecular interactions in IL-MS mixtures are quite different as compared to those in common organic solvents and this difference results in considerable change in the excited state dynamics of a dye molecule. For instance, the effect of the mixture composition of $HmimNTf_2$-ACN on the solvation dynamics of 12'CA was investigated. It was found a rise in the emission lifetime of the S_1 state with increasing mole fraction of ionic liquid, which was explained by stabilization of S_1 state due to increasing polarity of the corresponding IL-MS mixture.[49]

To sum up, there are many reports focused on unraveling the excited state properties of D149 in different molecular solvents;[24,30,32–35,49–51] however, to our best knowledge there is no any investigation of the excited state relaxation of D149 in IL-MS mixture. In our present work, we will fill the gap, and we are going to quantify the excited state relaxation times of D149 in the whole mixture composition range of aprotic solvent (acetonitrile), and 1-Butyl-3-methylimidazolium tetrafluoroborate ($BmimBF_4$) as well as in the neat components. The analysis of the dependence of these relaxation times on the composition, viscosity and polarity of the IL-MS mixture also allows us to assign them.

The paper is then organized as follow: in the second section we will give details on the experimental setup (stationary and time resolved ones) as well as on the data processing. In the third section, we will present and discuss the results and finally a conclusion is given in the fourth section.

2. EXPERIMENTAL SECTION

2.1. Chemicals:

The D149 dye (98%) and acetonitrile, ACN (≥ 99.9%, HPLC) were bought from Sigma Aldrich. The Imidazolium ionic liquid 1-butyl-3-methylimidazolium tetrafluoroborate, $BmimBF_4$ (≥ 98%) was bought from Solvionic. The ionic liquid and molecular solvent were stored under inert argon atmosphere to keep them away from the moisture. All binary solvents mixtures were prepared and kept inside the argon atmosphere glove box. The optical cuvettes were also filled with the samples inside the glove box just before the experiment to minimize the risk of introducing impurities. The structures of the ionic liquid and D149 dye are shown in Figure 1.

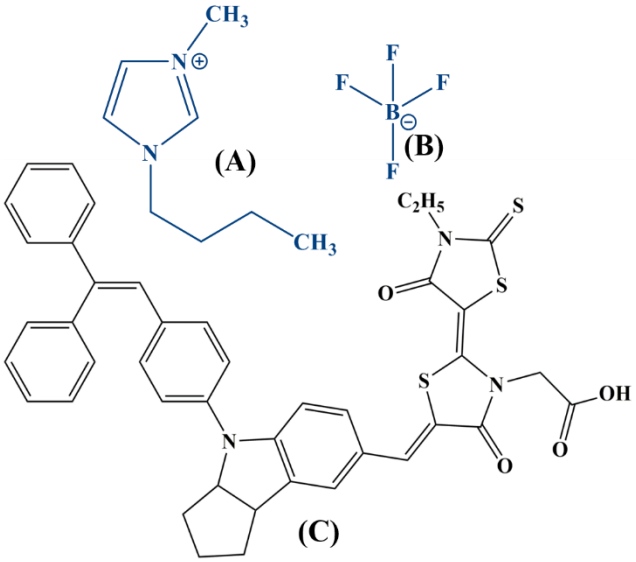

Figure 1: Structures of (A) Bmim cation, (B) BF_4 anion and (C) D149 dye.

2.1. Steady State Spectroscopy:

Steady state absorption and emission spectra of all samples were measured on Varian Cary 100 and on Jobin Yvon Fluoromax, respectively. 2 mm cuvettes were used for all the steady state measurements.

2.2. Femtosecond Transient Absorption (TA) Spectroscopy:

Femtosecond transient absorption setup used in this research has been described elsewhere.[52] First, the output of Coherent sapphire oscillator Micra 10 is amplified using Coherent Legend Elite. The output pulse (3.5 mJ and 45 fs time duration at 800 nm) is then divided into two pulses. The first, strong one (energy $\leq$ 15 μJ) passes through the optical parametric amplifier (Opera Solo) to create the pump pulse at 460 nm wavelength for the excitation of the sample. The second, weaker pulse goes through a CaF_2 crystal for the generation of white light supercontinuum probe pulse. After the excitation with the pump pulse, the delayed probe pulse passes through the same area of the sample and the transient absorption (TA) spectra is collected by using a spectrometer. The wavelength range of the probe beam for our experiment was chosen from 470 nm to 750 nm. The instrument response function (IRF) of the setup is 90 fs and it was calculated from the TA signal of pure acetonitrile in short delay range (this way pump-probe cross-correlation was detected and fitted using a Gaussian function).

2.3. Data Analysis:

After receiving the experimental TA time-resolved spectra, the first step is to perform global analysis. In this process, generally we refine the enormous amount of raw data into relatively small number of time independent spectra, each of them associated with a particular excited state process, characterized by a single time constant. The details are given in section 3.4.

3. RESULTS AND DISCUSSION

3.1. Steady state absorption and fluorescence spectra:

Steady state absorption and emission spectra of D149 in $BmimBF_4$-ACN mixtures are shown in Figure 2. The absorption spectra (red) contain two peaks corresponding to two different transitions-higher frequency S_0-S_2 and lower frequency S_0-S_1 with maxima at ~ 390 and ~ 530 nm, respectively.

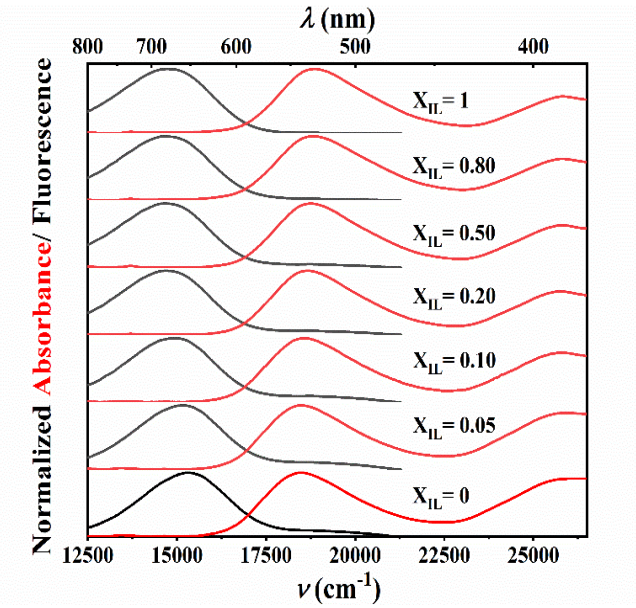

Figure 2: Normalized absorption and fluorescence spectra of D149 dye in $BmimBF_4$-ACN mixture at different mole fractions ($\lambda_{excitation}$= 460 nm).

According to the work of Le Bahers et al, both S_0-S_1 and S_0-S_2 absorption band were assigned to π-π^* transitions with charge transfer (CT) characteristics.[53] The S_0-S_1 band is red shifted in pure $BmimBF_4$ (λ_{Max}^{Abs} = 542 nm) compared to pure acetonitrile (λ_{Max}^{Abs} = 531 nm). There are some previous studies where a similar red shift of absorption maxima was observed in 12'CA molecule and other carotenoids in different organic solvents, ionic liquids and even in $HmimNTf_2$ and ACN binary mixtures and it was explained by the change of solvent polarizability defined by polarizability parameter (ΔR).[49,54–56] Recently, Zho et al. also reported similar red shift of absorption maxima of pyrene in N-butylpyridinium tetrafluoroborate-ACN binary mixture while increasing IL concentration.[57] They have discussed the effect of change of microstructure surrounding the dye and interactions between dye and ionic liquid alongside the effect of increasing viscosity as possible explanations for this behavior. Also, this red shift of absorption maxima of D149 was also seen in organic solvents.[30] All the values of absorption and emission maxima, polarity function (Δf) and polarizability function (ΔR) in our system are given in Table 1. It is clearly seen that, both the values of polarizability parameter (ΔR) of the medium and absorption maxima of the dye (λ_{Max}^{Abs}) rise with increasing mole fraction of ionic liquids in the mixture. While increasing ionic liquid mole fraction, the more polar excited state (μ_e = 36.54 D)[53] of the dye interacts stronger with the surrounding medium than the less polar ground state (μ_g = 19.22 D),[53] which eventually causes the gradual increase in red shift of the absorption maxima of the dye.

Table 1: Different steady state characteristics of D149 in $BmimBF_4$-ACN mixtures.

X_{BmimBF_4}	λ_{Max}^{Abs} (nm)	ν_{Max}^{Abs} (cm^{-1})	λ_{Max}^{Em} (nm)	ν_{Max}^{Em} (cm^{-1})	ν_{Stokes} (cm^{-1})	Δf*	ΔR*
0	531.0	18727.6	665.0	14442.1	4285.5	0.71	0.212
0.05	532.0	18648.0	666.0	14382.8	4265.2	0.70	0.213
0.10	534.0	18633.4	668.0	14409.8	4223.6	0.69	0.216

0.20	536.5	18539.5	667.0	14365.9	4173.6	0.68	0.219
0.50	539.5	18446.9	659.0	14540.3	3906.6	0.63	0.230
0.80	542.0	18378.4	649.5	14799.0	3579.4	0.59	0.241
1	542.5	18353.5	644.0	15025.1	3328.4	0.57	0.247

* $\Delta f = (\varepsilon-1)/(\varepsilon+2)-(n^2-1)/(n^2+2)$, $\Delta R = (n^2-1)/(n^2+2)$, here ε and n are the values of dielectric constants[17] and refractive indices[17] of the binary mixtures of different compositions

The emission spectra (Figure 2, black) of D149 corresponds to S_1-S_0 transition and this is red-shifted compared to the absorption band. Emission band has a very weak vibronic shoulder.[34] Emission maxima positions show an overall blue shift while decreasing the polarity of the solvent mixture ($\lambda_{\mathrm{Max}}^{\mathrm{Em}}$ = 644 nm in $BmimBF_4$ while $\lambda_{\mathrm{Max}}^{\mathrm{Em}}$ = 665 nm in acetonitrile) (Table 1, Figure 3(A)). However, the initial red shift ($X_{IL} \leq 0.1$) of emission maxima is an indication of stabilization of excited state in the dye. In general, the emission maxima values of dye are sensitive to local environment. Therefore, this initial red shift could be due to some interactions between the dye and the surrounding medium.

In Figure 3(B), the changes of Stokes shift in D149 are shown with respect to X_{IL} in the $BmimBF_4$-ACN binary mixtures. The Stokes shift decreases with increasing mole fraction of ionic liquid. According to Lohse et al., the increase of Stokes shift for D149 in pure solvents is due to the medium polarity.[30] The solvatochromic polarity parameter (E_N^T) of $BmimBF_4$ is higher than that of polar aprotic ACN.[58–60] According to a previous report by Manchini et al., E_N^T values of $BmimBF_4$-ACN mixtures also increased while increasing X_{IL};[61] however, in case of ionic liquids, polarity of the medium is not so easy to describe. According to Wakai et al.,[18] the concept of polarity in ionic liquids is different than that of conventional solvents due to presence of charged species in the medium. Stoppa et al.[17] measured dielectric constant (ε) of $BmimBF_4$-ACN binary mixture at different IL mole fractions using dielectric relaxation spectroscopy (DRS). Although there was an initial increase at very low X_{IL} of $BmimBF_4$ ($X_{IL} \leq 0.01$), overall values of ε show a gradual decrease from pure ACN to pure $BmimBF_4$. Indeed, our Stokes shift data show the correlation with Δf calculated from dielectric constant (ε) values instead of spectroscopic polarity parameter E_N^T values calculated in $BmimBF_4$-ACN mixtures. As the values of polarity parameter (Δf) decrease, the Stokes shift values of the dye in $BmimBF_4$-ACN binary mixtures also decrease while increasing ionic liquid mole fractions, although the correlation is not linear.

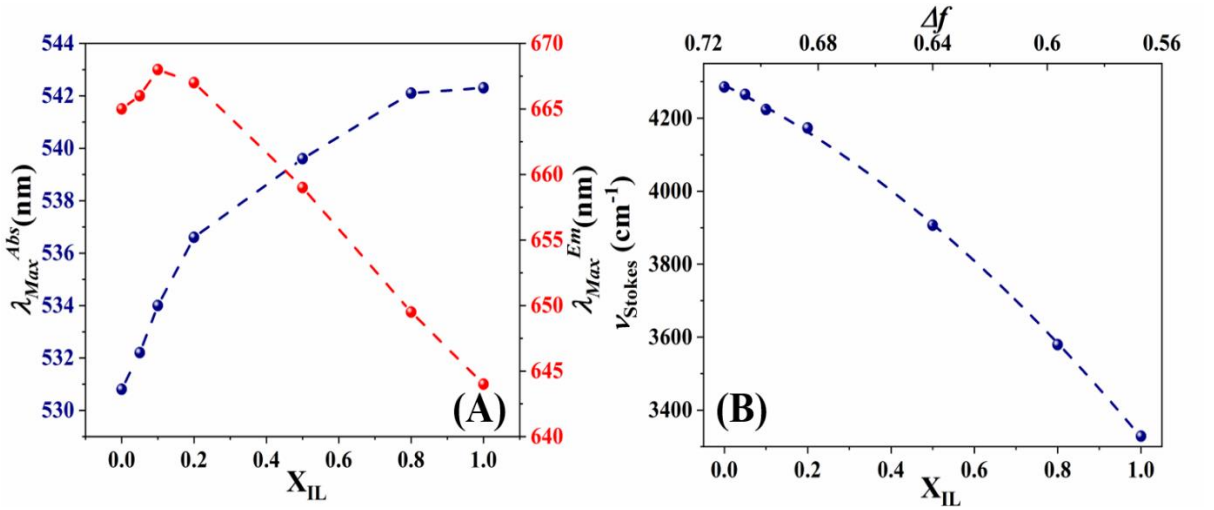

Figure 3: (A) Change of absorption and emission maxima and (B) change of Stokes shift against mole fraction of ionic liquid in $BmimBF_4$-ACN binary solvent mixture.

3.2. Relative Quantum Yield:

From the steady state absorption and emission spectra, we can get an idea about relative quantum yield of the dye in solvent mixtures, which can be expressed as the area under the emission spectra normalized with respect to absorption at excitation wavelength of 460 nm. Previously relative quantum yield was shown in case of D149 in pure solvents by El-Zohry et al.[33] In Figure 4, we can see the change of relative quantum yield of the dye D149 with IL mole fraction in $BmimBF_4$-ACN mixture.

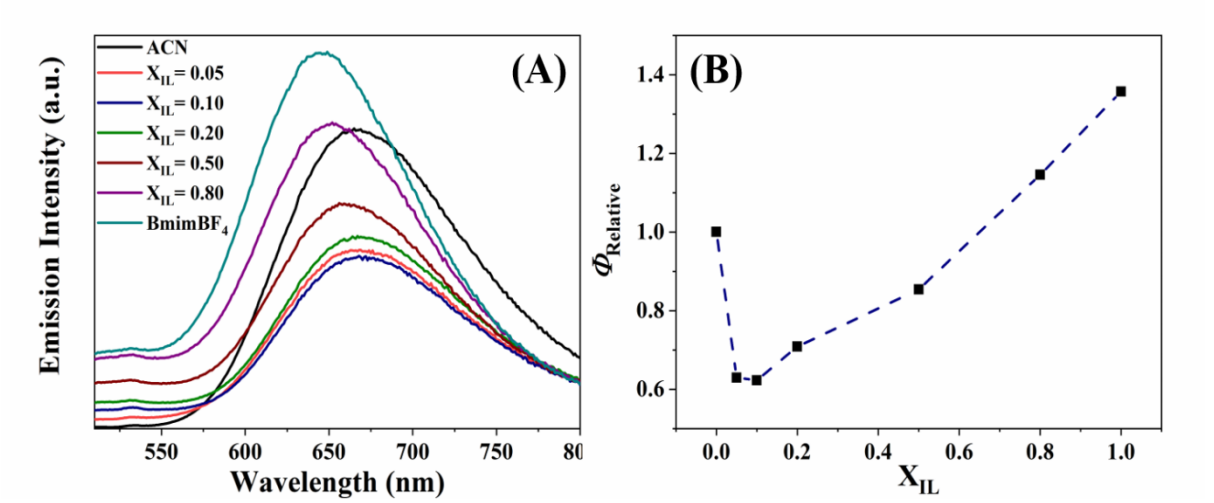

Figure 4: (A) Emission intensities normalized to absorption at $\lambda_{excitation}$ (460 nm) in $BmimBF_4$-ACN binary mixtures, (B) areas under the curve in panel (A) (i.e. relative quantum yield).

Quantum yield (relative quantum yield in our case) gives the idea about the relaxation of the excited state in the dye to its ground state. In Figure 4(B), an overall increase of $\phi_{relative}$ is seen while increasing $BmimBF_4$ mole fraction; however, there is an initial decease at very low X_{IL} ($X_{IL} \leq 0.1$). The relative quantum yield value is highest for pure $BmimBF_4$. We have set the value of $\phi_{Relative}$ in ACN to 1 to get an idea of its change with different mole fractions of ionic

liquid, the reported experimental quantum yield of D149 in ACN is 4.64%.[34] While interpreting the dependence of ϕ_{relative} on the mole fraction, we have to keep in mind that, we are decreasing polarity[17] and increasing viscosity[15] of the medium by increasing X_{IL}. It was previously documented by Lohse et al. that, S_1-S_0 transition is dominated by internal conversion (IC) with minor contribution of radiative decay.[30] The decrease in polarity of the medium results in a smaller contribution of the non-radiative IC to the deactivation of S_1, which will eventually increase the value of quantum yield. In the higher mole fraction region of ionic liquid, the viscosity change is very high as compared to polarity change of the medium. Unlike polarity, viscosity of $BmimBF_4$-ACN binary mixture increases while increasing mole fraction of $BmimBF_4$. Previous report suggested an increase of lifetime of D149 due to blocked internal motion of the dye in highly viscous solvents.[34] This damping of internal motion results in decreasing the non-radiative decay process and as a result, ϕ_{relative} values rise while increasing X_{IL}. Therefore, both polarity and viscosity of the mixture help to explain the overall increase of the relative quantum yield at larger X_{IL}; however, the minimum at X_{IL} = 0.1 might indicate some kind of interaction between the dye and the medium which eventually increase the rate of non-radiative decay processes.

Overall, the steady state results suggest that, at X_{IL} = 0.1 the emission maximum position is highest (668 nm in Table 1) while ϕ_{relative} is lowest. The highest $\lambda_{\text{Max}}^{\text{Em}}$ value suggests lowest S_1-S_0 energy gap, which seems opposite to the lowest ϕ_{relative} value apparently. This can be explained considering the fact that, decreasing S_1-S_0 energy gap increases the rate of non-radiative IC process which eventually results in lower ϕ_{relative} value.[30,49] A minimum at X_{IL} = 0.1 also occurs in the values of emission lifetime after TA global analysis, which will be discussed later while discussing transient absorption results.

3.3. Femtosecond Transient Absorption spectroscopy:

With the goal to study the excited state dynamics of D149 dye in IL-MS mixture at different IL mole fractions, femtosecond transient absorption measurements were performed. Based on the time-integrated absorption measurements, the excitation maximum at 460 nm was chosen in order to excite the dye to its first excited (S_1) state. For better comparison of the results, similar excitation wavelength was used to excite all the samples. The measured probe wavelength region was from 470 nm to 750 nm.

All the transient absorption spectra of D149 in $BmimBF_4$-ACN binary mixtures are shown in Figures 5 and S1-S6. First, we are going to discuss different spectral features in transient absorption data for D149 in pure $BmimBF_4$.

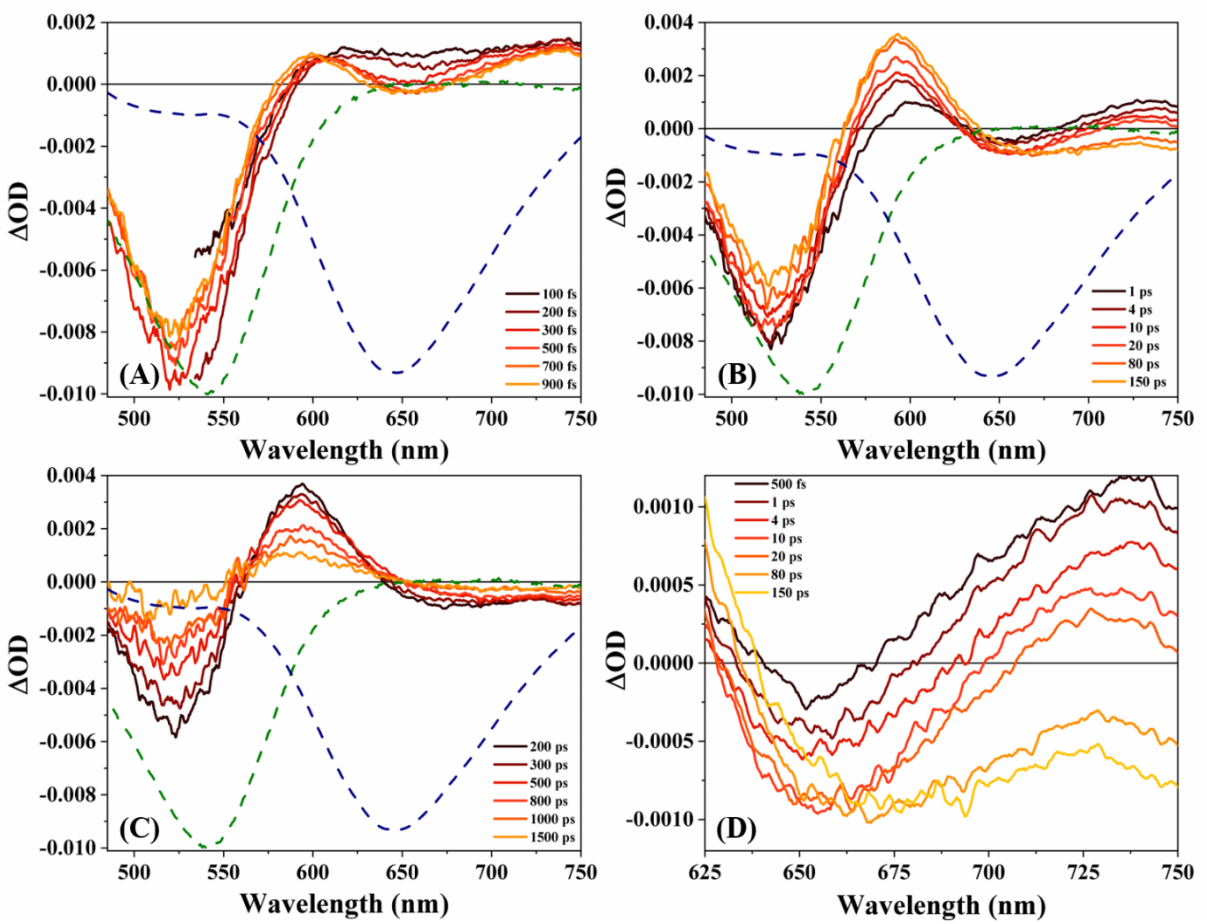

Figure 5: Transient Absorption spectra of D149 in $BmimBF_4$, (A) short timescale (100-900 fs), (B) middle timescale (1-150 ps), (C) long timescale (200-1500 ps), (D) solvation timescale. Dashed spectra are steady state absorption (green) and emission (blue) spectra.

To make the analysis of the transient absorption spectra (TAS) of D149 in $BmimBF_4$, we have split the data into three different time regions (Figures 5A-C).

In Figure 5(A), first a negative (ground state bleach (GSB)) band appears due to the depopulation of ground state (S_0) which leads to the population of the excited state (S_1) in the D149 dye. Furthermore, the spectral overlap between the time-integrated absorption and GSB indicates that the latter is a result of S_0-S_1 absorption. The bleach band increases within the first 400 fs and then its intensity starts decreasing due to the recovery of the ground state. Also, in 550-750 nm region, the transient absorption signal is positive due to excited state absorption (ESA) from the excited (S_1) state. Within 1 ps, the positive ESA band with maximum at 600 nm starts increasing while its part above 650 nm starts decreasing.

In Figure 5(B), we observe gradual reduction of the GSB band with the increase of pump-probe time delay as a result of recovery of S_0 state. At the same time, ESA with the maximum at 600 nm gradually increases within few teens of ps due to geometry relaxation *(vide infra)*. After 20 ps, the positive band between 650-750 nm becomes negative. The comparison of transient absorption spectra with time-integrated absorption and emission suggests that the contribution of the negative signal in the range of 650-750 nm results from stimulated emission from S_1 to S_0. At the beginning, the signal within this region was positive because of the excitation which results in a population of higher vibronic levels in S_1 and/or in a population of

geometrical form of D149, both dissipating non-radiatively the excess energy, giving rise to the low vibronic level emitting form. The negative signal rises within few teens of picoseconds similar to ESA. As both ESA and SE characterize the S_1 state, the observed rise is due to geometry relaxation of D149.[30] Hence, the initial ultrafast decay of positive signal in the region of SE is dominated by vibrational and geometrical relaxation of the dye.

In both Figures 5(A) and 5(B), first we observe the excited state absorption on the ultrafast timescale followed by the stimulated emission. Moreover, the reduction of D149 excited state due to geometry and vibrational relaxation results in a shift of emission maximum towards longer wavelengths, and thus the minimum in transient absorption spectra appears at approximately 660 nm (Figure 5(D)).

Finally, in Figure 5(C), we can see the reduction of transient absorption spectra in the whole spectral region due to S_1-S_0 transition which is in agreement with previous reports *(vide infra)*.[30,32] Although the TAS of D149 in pure ACN and in the binary mixtures with $BmimBF_4$ have almost similar characteristics to the TAS of D149 in $BmimBF_4$, there is a slight difference. In Figures S1(B)-S6(B), the rise in ESA and SE bands of D149 is shorter in the binary mixtures and in pure ACN than in pure $BmimBF_4$. This is mainly due to faster geometry relaxation of excited state in the dye related to the decreasing viscosity of the surrounding medium.

We have also studied the effect of composition change on TA spectra. Of note is that Figures S1-S6 illustrate the D149 relaxation in a mixture which viscosity and polarity (as quantified by the experimental dielectric constant) are modulated by the mixture composition. The polarity is increasing when adding ACN to BmimBF4 while the viscosity decreases. The shape of the ESA for D149 in ACN, is similar to that published by Lohse et al.[37] Two main spectral regions characterize the relaxation of the D149 in the studied mixture. The one located between 488 nm and 588 nm is associated with the GSB. The position of crossover region of the GSB and ESA is dependent on the mixture composition and on the time evolution of the TAS. The second spectral region is located between 588 nm and 750 nm and is characterized by a strong overlap between the ESA that covers this whole spectral region at early times and the SE that is characterized by a deepening around 652 nm, the extent of which is both time and mixture composition dependent. The SE contribution is red shifted as it is illustrated in panel D of Figures 5 and S1-S6. This shift determines to a large extent the structuration of the shape of the ESA into one or two spectral contributions centered at 599 nm and 734 nm, respectively. Lohse et al. noticed that the intensity of the lower wavelength contribution is high in polar solvent such as ACN and MeOH, while that of the higher wavelength contribution is reduced. This is a result of the increase of the spectral overlap between the higher wavelength ESA and the SE contribution because of the gradual redshift of the SE band. In less polar solvent such as THF, Lohse et al.[30] shows that the SE signal emerges at lower wavelength than that of the ESA observed at higher wavelengths. As a result, this contribution remains visible in this solvent. The evolution of the shape of ESA as a function of X_{IL} is consistent with this interpretation. Indeed, in neat ionic liquid that is characterized by a low polarity (compared to that of ACN), the two contributions in the ESA are well resolved while in neat ACN the component at higher wavelengths is not visible. The time and X_{IL} dependence of the SE shift is illustrated at a chosen delay time 500 fs, 1 ps, 30 ps and 150 ps in Figure 6. It shows that the SE contribution is dependent on the polarity of the mixture. It is located at shorter wavelength as compared to that in ACN. As a consequence, the highest wavelength ESA contribution decreases with increasing

ACN content in the mixture. Concomitantly the ratio between the contributions of ESA located at shorter and longer wavelengths is increasing. These differences in the shape of TA spectra at different pump-probe time delays (500 fs-150 ps) suggest the influence of the surrounding medium on the geometry/energy of the photoexcited dye molecule.

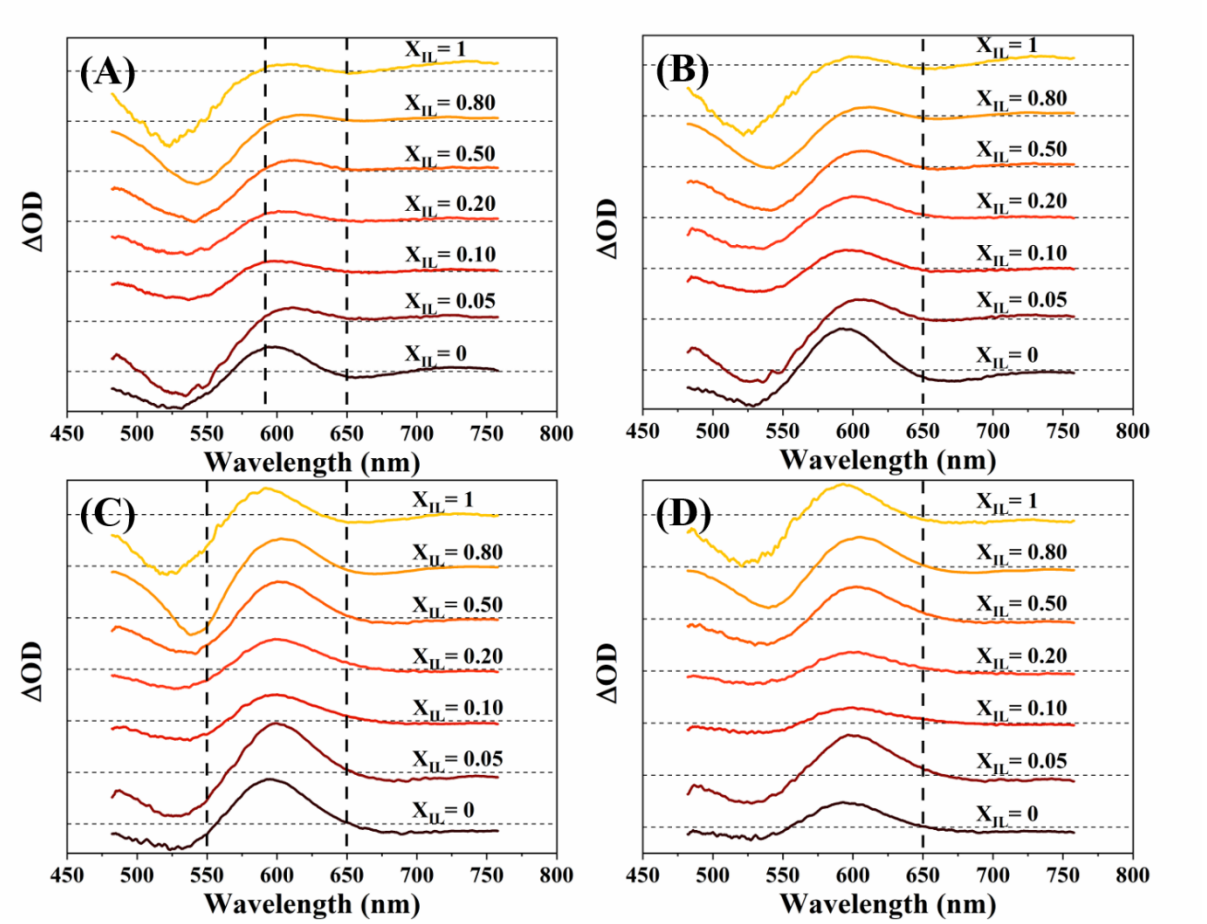

Figure 6: Transient absorption spectra of D149 in pure ACN, $BmimBF_4$ and their binary mixtures at different times [(A) 500 fs, (B) 1 ps, (C) 30 ps and (D) 150 ps].

3.4.Global analysis of transient absorption data:

The global analysis of the transient absorption data was carried out using a MATLAB based tool called ultrafast Toolbox.[62] In that case, the transient absorption signal is described as a sum of first order processes each characterized by a rate constant k_i.

$$\Delta A(t) = I_0 + \int_{-\infty}^{\infty} dt' \sum_{i=0}^{m} A_i(\lambda) e^{-k_i t'} I_{rf}(t - t') \quad (1)$$

Where I_0 is the offset, m is the number of processes and I_{rf} is the instrumental response function (IRF)

$$I_{rf}(t) = \exp\left(-\left(\frac{t}{\tau_{irf}}\right)^2\right) \quad (2)$$

The IRF is obtained from the transient absorption signal of pure acetonitrile on very fast timescale where τ_{irf} is the instrument response time. The wavelength dependent pre-exponential factor $A_i(\lambda)$ forms a separate time independent decay associated spectrum (DAS) for each rate constants k_i, that corresponds to a decay time $\tau_i = (k_i)^{-1}$.

There are previous reports suggesting that for D149 in pure ACN and in other organic solvents, the global analysis of transient absorption spectra results in a good fit when four components are used.[30,32,34] Our analysis of all the TA spectra of D149 in different solvents starting from pure ACN to pure $BmimBF_4$ also leads us to four different time components which are shown in Table S1. To learn about the nature of these time constants, we need to take a closer look on the DAS related to each of them, which is discussed in the next section.

3.5. Decay Associated Spectra (DAS):

In Figures 7 and S13-S17, all the DAS of D149 in different solvents are shown. For the discussion, we focus on DAS of D149 in ACN (Figure 7(A)) and $BmimBF_4$ (Figure 7(B)) only. We can cover the other DAS also by discussing these two.

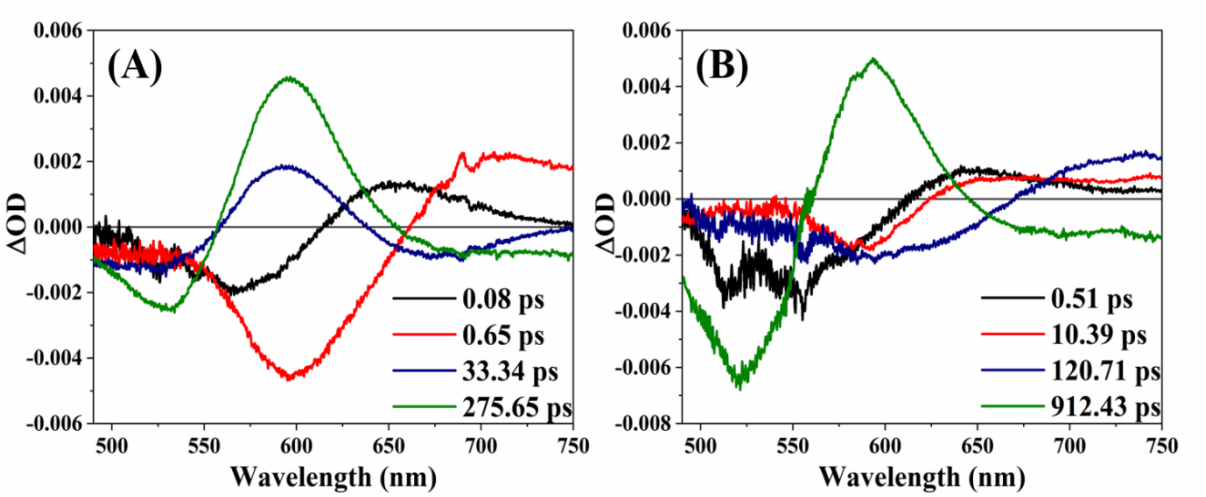

Figure 7: Decay Associated Spectra of D149 in (A) Acetonitrile and (B) $BmimBF_4$.

In Figure 7, the spectra related to longest time component (τ_4, green) show almost similar characteristics (negative GSB and SE, positive ESA). The DAS related to two comparatively smaller time components (τ_1 and τ_2, black and red) show opposite signs compared to the spectra related to τ_4 (mainly in the ESA and SE regions), which indicates that both τ_1 and τ_2 are rise components. Also, the characteristic shift between these two spectra of τ_1 and τ_2 in the longer wavelength region shows that they can be attributed to solvation dynamics. However, the behavior of the DAS associated with τ_3 is different in the case of ACN and $BmimBF_4$. In pure $BmimBF_4$ and in its mixtures with ACN (Figures S13-S17), the τ_3 spectra show similar behavior to τ_1 and τ_2 (i.e. opposite sign to τ_4 in ESA and SE region of TA). Thus, the τ_3 can originate from processes in the excited state which are not related to the decay to the ground state. In contrary, the τ_3 DAS for D149 in ACN has the same sign as the one of τ_4. Thus, it can be associated with decay process of some short-lived populations of excited (S_1) state of the dye that could correspond to a different geometry for example.

3.6. Fitted kinetic traces:

In Figures 8 and S7-S12, we have plotted the representative kinetic traces with their fits from global analysis at three different wavelengths of the transient absorption spectra of D149 in pure $BmimBF_4$, ACN and their binary mixtures at different IL content. The wavelengths were chosen to show dynamics within representative spectral ranges of TA spectra (GSB, ESA and SE). As the traces are almost similar, describing the traces of D149 in $BmimBF_4$ will be enough to understand other.

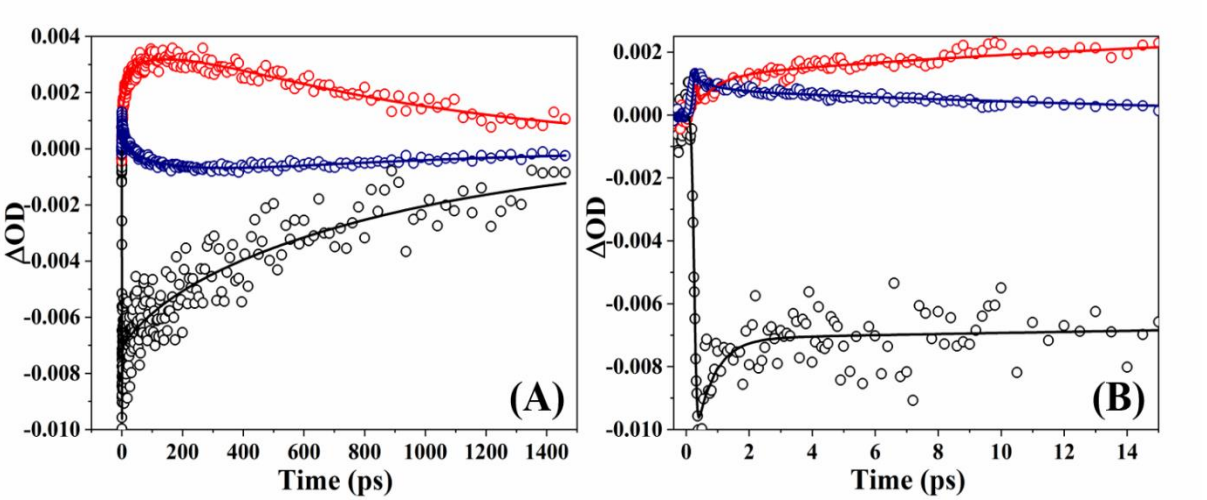

Figure 8: Experimental (hollow circles) and fitted (line) kinetic traces of D149 in $BmimBF_4$ at different wavelengths 525 nm (black), 600 nm (red) and 720 nm (blue) of TA spectrum. (A) long timescale (0-1.5 ns), (B) short timescale (0-15 ps).

In Figure 8(A), the TA decay at 525 nm for D149 in pure $BmimBF_4$ is shown. This wavelength falls in the GSB region of the TA spectra and it shows a sharp rise of negative signal and then a recovery with time constant corresponding to the emission lifetime of 912.43 ps in case of $BmimBF_4$. We can see an additional fast decay at very short times (Figure 8(B)) and this is due to solvation dynamics of the medium. At 600 nm, the trace shows S_1-S_n ESA and at 720 nm, there is an overlap between S_1-S_n ESA and S_1-S_0 SE (Figure 8(A)). The final decay at 600 nm and 720 nm is also due to the repopulation of S_0 state. In Figure 8(B), also for these two wavelengths we can see an initial rise due to the solvation dynamics. These initial rises are different in the kinetic traces of D149 in different binary mixtures and in pure ACN (Figures S7(B)-S12(B)), which indicates that this process is dependent upon different properties (polarity, viscosity) of the medium surrounding the dye.

3.7. Discussion of Four Global Analysis Time Constants:

As mentioned before, the four time components describe the D149 relaxation at various mixture compositions. The values in ACN are consistent with the literature data on the D149 in this solvent. Of note is that in the case of $\tau_1$and τ_2, similar values were reported for D149 in various solvents such as tetrahydrofuran (THF), dichloromethane (DCM), acetone (ACT), ethanol (EtOH) and methanol (MeOH)[30,34] and also for similar dyes having almost the same structure such as D102 and D131. The two shorter time components τ_1 and τ_2 were assigned to

the solvent relaxation as reported in a seminal work by Maroncelli[43] and they were evidenced in the relaxation process of many dyes including the D149.[30,34] Furthermore, El-Zohry et al. assigned these relaxation times to the intramolecular vibrational redistribution (IVR).[34] In that study the relaxation process of only the donor moiety of the D149 was analyzed and the authors reported that in D149 the IVR relaxation time is around 0.09 ps, while in the case of D131 dye it is increased to 0.6 ps. Another assignment was suggested by Ziolek et al., who reported that initially the dye is excited to a local excited state, which then relaxes to the charge transfer state within the first 1 ps.[63]

The τ_1 and τ_2 values are shown as a function of both the polarity and viscosity of the mixtures of different IL concentrations in Figure 9. The values of these relaxation times increase with decreasing the polarity of the solvent.

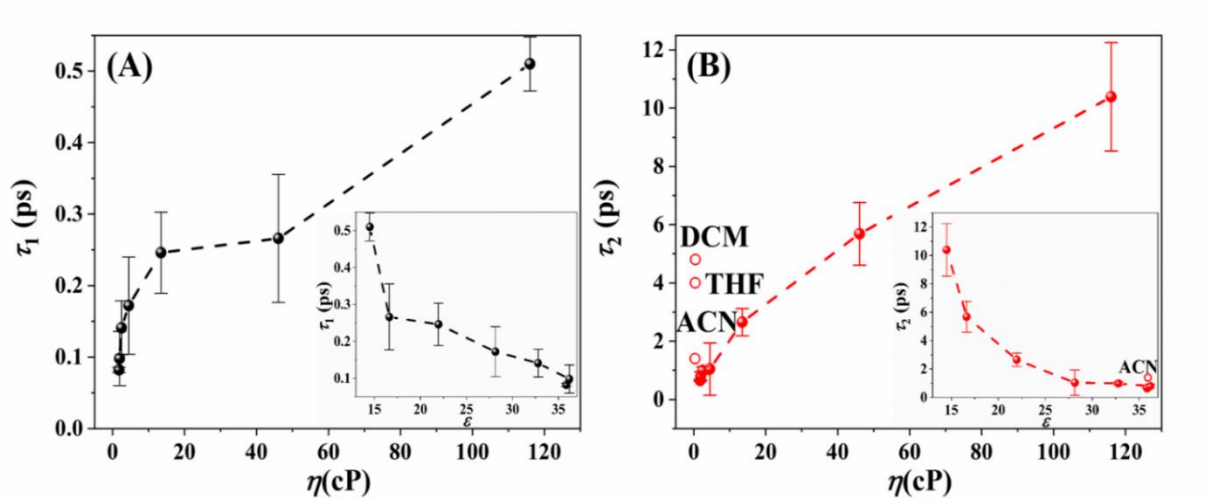

Figure 9: Viscosity and polarity (inset) dependence of (A) τ_1 and (B) τ_2 relaxation times in the mixture of $BmimBF_4$ and ACN. Previous published values are shown in open circles. [30,32,34,51]

The viscosity dependence is stronger for τ_2 (16x increase) than for τ_1 (6x increase) and is close to linear for the former. This indicates that τ_2 process might involve solvent dynamics or structural relaxation, which should follow the Stokes-Einstein-Debye (SED) equation.[41] On the other hand, intramolecular processes like IVR can depend on polarity, which in the case of τ_1 results in nonlinear viscosity dependence. A factor analysis on a broader data set is needed to precisely disentangle the possible contribution of both viscosity and polarity dependence of τ_1 and τ_2.

The τ_3 relaxation time is more problematic and will be discussed as the last one. Turning now to the slowest relaxation time τ_4 there is a large convergence on its interpretation as being associated with the lifetime of the S_1 state. The literature data shows that τ_4 is strongly dependent on the solvent polarity, viscosity, dye concentration and also the hydrogen bonding between the dye and the protic solvents.[32,34] Increasing the concentration of the dye and the formation of hydrogen bonding induces a faster deactivation.

If we describe the solvent by its viscosity and polarity values, we can compare the τ_4 values for the D149 dye in $BmimBF_4$-ACN system and in various pure solvents.[35,51] Of note is that the merit of our work is to explore larger values of the viscosity than reported in the literature. As it is illustrated in Figure 10(B), when the environment of the D149 is characterized

by its macroscopic polarity and viscosity, the excited state lifetime as quantified by τ_4 values increases with decreasing the former and increasing the later parameter.

We thus expect that the origin of 3-fold increase (Table S1) in τ_4 when going from pure ACN to pure IL is due to (i) increased viscosity, which slows down the relaxation due to double bond twist between the donor and acceptor units,[32,33] (ii) decreased polarity, which decreases the non-radiative ICT process related to S_1-S_0 decay. Indeed, previous papers[30,32] showed that the values of emission lifetime of D149 increase while decreasing the polarity of different organic solvents. In our case, the values of static dielectric constant (ε), which is directly related to solvent polarity, is smaller in case of pure $BmimBF_4$ (ε = 14.6) than for ACN (ε = 35.84).[17] This clearly suggests that, polarity of the medium surrounding the dye molecule is also a reason of the increased lifetime of D149 while going from pure ACN to pure $BmimBF_4$. This limiting of the non-radiative relaxation processes is also reflected in the higher quantum yield in pure IL.

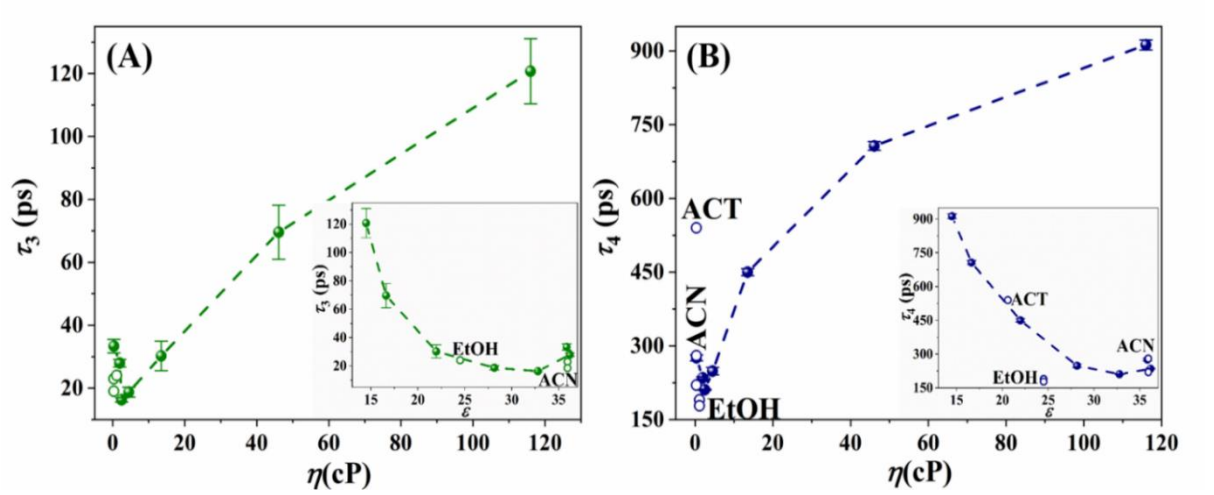

Figure 10: Viscosity and polarity (inset) dependence of (A) τ_3 and (B) τ_4 relaxation times in the mixture of $BmimBF_4$/ACN mixture. These values are compared with those obtained for neat solvents-open green circles for τ_3 and open blue circles for τ_4. [30,32,34,51]

From figure 10(B), it is evident that, τ_4 do not quite follow the change in viscosity and polarity (measured by dielectric constant) of the surrounding medium in the lower mole fraction region of ionic liquid. Our classical MD simulation analysis of the mixture shows that between X_{IL} = 0 and X_{IL} = 0.1, a transition occurs from the situation where the local structure is dominated by that of the solvent to the one dominated by the ionic liquid. Indeed, in this range of X_{IL}, the average distances, between the ions, the ions and the solvent molecules, as calculated by the nearest neighbor radial distribution undergo a crossover.[64]
Therefore, we suggest that the minimum value at X_{IL} = 0.1 (Table S1) is due to a joint effect of interaction with the two components of the mixture that leads to increased contribution of the non-radiative decay pathways, which is also reflected by the minimum in quantum yield.

The behavior of the τ_3 is illustrated in Figure 10(A). This relaxation time is systematically found when analyzing the decay relaxation of the D149 in various neat solvents having either the polarity or viscosity in the same range as those of the $BmimBF_4$/ACN mixture.[30,32,34,51] The assignment of this relaxation time is controversial as it is indicated by the literature data on the D149 dye. Lohse et al. tentatively assigned it to collisional cooling or

structural S_1 relaxation.[30] El-Zohry et al.[34] proposed that this relaxation time cannot be assigned to solvent relaxation as its values in many neat solvents are higher than the solvent relaxation time. They showed that the oscillator strength of different excited states is significantly affected by rotation of either the single or double bond between the acceptor and donor parts, which can favor local excitation at the donor unit for some geometries of the dye and thus result in two populations with different excited state lifetimes. They conducted a systematic study to understand the origin of this relaxation time that is also observed in D102 and D131 dyes, and assigned it to the ultrafast twisting of the diphenyl vinyl group in the donor unit that is present in the three dyes.

In the case of pure IL and IL/MS mixtures, the τ_3 DAS shape suggests that it involves solvation dynamics and/or structural relaxation. Chowdhury et al. had also found a solvation time constant of 60 ps in $BmimBF_4$ using C153 dye.[50] Indeed, in our recent optical Kerr effect study of a similar $BmimPF_6$/ACN mixture (bulk solvent without the dye) we showed that admixing IL to acetonitrile results in a significant slow-down of the mixture dynamics. We observed that already at X_{IL} = 0.05, the slowest relaxation time is 18 ps and grows to 1.6 ns for pure IL.[65] In the case of systems with the dye, these relaxation times might differ in the cybotactic region compared to the bulk; however, they clearly show that solvation can be involved in τ_3. In our case even for pure IL we cannot see any evidence of solvation in the DAS associated with τ_4, while it is clearly observed for τ_3 for pure IL and all the mixtures. For IL-MS mixtures, the shape of τ_3 DAS shows no clear indication of decay characteristics. Nevertheless, in Figure 10(A) we can see that the viscosity and polarity dependence of τ_3 is similar to that of τ_4, therefore a mix of solvation and decay might be involved.

Although the shape of the DAS of D149 in our study suggests the presence of a decay channel of a short-lived species in pure ACN, attributing τ_3 to decay of such short-lived excited state is contradictory. As discussed by El-Zohry et al.,[34] may be some twisted, locally excited, short-lived populations of the dye are present only in case of pure ACN, which are the reason for this decay character of the DAS of τ_3 in pure ACN; however, it is not clear why the τ_3 DAS shows no indication of decay character in $BmimBF_4$-ACN mixtures, even at very low IL content (X_{IL} = 0.05). Thus, in order to get further insights regarding the interpretation of this timescale, we are planning to carry out molecular modeling to get information about the relaxation dynamics of D149 (relaxation time of twisting process of the dye, hydrogen bonding between dye and the components of IL-MS mixture).[66–68]

In summary we can conclude that, for pure IL the origin of τ_3 is mainly due to solvation, whereas in case of pure ACN, the origin of τ_3 remains contradictory. Moreover, this relaxation time is affected by the decrease/increase of the polarity/viscosity of the D149 dye environment in a very similar fashion as τ_4, i.e. the relaxation time.

4. CONCLUSIONS

In this work, we have studied the dynamics of the excited state of D149 dye in $BmimBF_4$-ACN binary mixtures for the very first time using steady state and transient absorption spectroscopy. The steady state Stokes shift values show their dependence upon the mixture polarity. Using global analysis of the experimental transient absorption spectra of the excited state of D149 dye, four different time components were found related to different excited state processes. Two

comparatively smaller constants (τ_1, τ_2) are related to solvation dynamics and IVR and the values increase with the increase of both polarity and viscosity of the binary mixtures. Although the viscosity dependence of τ_2 follows SED relation, τ_1 does not change linearly with the viscosity of the surrounding medium, which suggests the IVR characteristics of the later. The longest time component (τ_4) is related to the emission lifetime and is correlated with both the polarity and viscosity of the medium. However, the initial decrease of τ_4 in lower X_{IL} region, which is also noticed in the relative quantum yield values, indicates the presence of interactions between dye molecules and the mixture, which eventually increases the contribution of non-radiative pathways leading to the decrease of emission lifetimes. DAS analysis helped us to investigate the origin of another moderately slow time constant (τ_3). In case of pure $BmimBF_4$ and its mixtures with ACN, this timescale has solvation characteristics, as the DAS shape of τ_3 is similar to τ_2. However, in case of pure ACN, the origin of τ_3 remains contradictory. Further theoretical calculations are needed to get a detailed picture of the excited state relaxation of the dye. Moreover, we noticed that the polarity and viscosity dependence of τ_3 is similar to τ_4. Our study also provides the mixture composition dependence of the excited state relaxation times of an organic sensitizer used in DSSC. Further studies should be carried out to quantify the mixture dependence of the other processes to optimize the working optimal conditions of the solar cell.

5. ASSOCIATED CONTENTS

Global analysis time constants of D149 in $BmimBF_4$-ACN mixtures, transient absorption spectra of D149 in pure ACN and in different compositions $BmimBF_4$-ACN mixtures (Figures S1-S6), experimental and fitted time traces of D149 in pure $BmimBF_4$ and in different compositions of $BmimBF_4$-ACN mixtures (Figures S7-S12), All the DAS of D149 in different compositions of $BmimBF_4$-ACN mixtures (Figures S13-S17)

6. ACKNOWLEDGEMENTS

The authors acknowledge financial support from the Polish National Agency for Academic Exchange (project No. PPN/BIL/2018/1/00207/U/00019) and the French Intergovernmental Science and Technology Program Polonium (project No. 42706QK) and the French National Agency for Research (ANR-19-CE05-0009-01 Ultrafast photoinduced processes of organic dyes in ionic liquid/molecular solvent mixtures designed for dye solar cells). PP acknowledges the support from National Science Centre (Poland) through project No. 2017/26/D/ST3/00910.

7. CONFLICTS OF INTERESTS

There are no conflicts of interest to declare for this study.

REFERENCES

(1) O'Regan, B.; Grätzel, M. A Low-Cost, High-Efficiency Solar Cell Based on Dye-Sensitized Colloidal TiO2 Films. *Nature* **1991**, *353* (6346), 737–740. https://doi.org/10.1038/353737a0.

(2) Yella, A.; Lee, H.-W.; Tsao, H. N.; Yi, C.; Chandiran, A. K.; Nazeeruddin, M. K.; Diau, E. W.-G.; Yeh, C.-Y.; Zakeeruddin, S. M.; Gratzel, M. Porphyrin-Sensitized Solar Cells with Cobalt (II/III)-Based Redox Electrolyte Exceed 12 Percent Efficiency. *Science (80-.).* **2011**, *334* (6056), 629–634. https://doi.org/10.1126/science.1209688.

(3) Eom, Y. K.; Kang, S. H.; Choi, I. T.; Yoo, Y.; Kim, J.; Kim, H. K. Significant Light Absorption Enhancement by a Single Heterocyclic Unit Change in the π-Bridge Moiety from Thieno[3,2-b]Benzothiophene to Thieno[3,2-b]Indole for High Performance Dye-Sensitized and Tandem Solar Cells. *J. Mater. Chem. A* **2017**, *5* (5), 2297–2308. https://doi.org/10.1039/C6TA09836C.

(4) Mathew, S.; Yella, A.; Gao, P.; Humphry-Baker, R.; Curchod, B. F. E.; Ashari-Astani, N.; Tavernelli, I.; Rothlisberger, U.; Nazeeruddin, M. K.; Grätzel, M. Dye-Sensitized Solar Cells with 13% Efficiency Achieved through the Molecular Engineering of Porphyrin Sensitizers. *Nat. Chem.* **2014**, *6* (3), 242–247. https://doi.org/10.1038/nchem.1861.

(5) Wu, J.; Lan, Z.; Lin, J.; Huang, M.; Huang, Y.; Fan, L.; Luo, G. Electrolytes in Dye-Sensitized Solar Cells. *Chem. Rev.* **2015**, *115* (5), 2136–2173. https://doi.org/10.1021/cr400675m.

(6) Wu, J.; Lan, Z.; Hao, S.; Li, P.; Lin, J.; Huang, M.; Fang, L.; Huang, Y. Progress on the Electrolytes for Dye-Sensitized Solar Cells. *Pure Appl. Chem.* **2008**, *80* (11), 2241–2258. https://doi.org/10.1351/pac200880112241.

(7) Sugathan, V.; John, E.; Sudhakar, K. Recent Improvements in Dye Sensitized Solar Cells: A Review. *Renew. Sustain. Energy Rev.* **2015**, *52*, 54–64. https://doi.org/10.1016/j.rser.2015.07.076.

(8) Robertson, N. Optimizing Dyes for Dye-Sensitized Solar Cells. *Angew. Chemie - Int. Ed.* **2006**, *45* (15), 2338–2345. https://doi.org/10.1002/anie.200503083.

(9) Le Bahers, T.; Labat, F.; Pauporté, T.; Lainé, P. P.; Ciofini, I. Theoretical Procedure for Optimizing Dye-Sensitized Solar Cells: From Electronic Structure to Photovoltaic Efficiency. *J. Am. Chem. Soc.* **2011**, *133* (20), 8005–8013. https://doi.org/10.1021/ja201944g.

(10) Bella, F.; Nair, J. R.; Gerbaldi, C. Towards Green, Efficient and Durable Quasi-Solid Dye-Sensitized Solar Cells Integrated with a Cellulose-Based Gel-Polymer Electrolyte Optimized by a Chemometric DoE Approach. *RSC Adv.* **2013**, *3* (36), 15993. https://doi.org/10.1039/c3ra41267a.

(11) Kawano, R.; Matsui, H.; Matsuyama, C.; Sato, A.; Susan, M. A. B. H.; Tanabe, N.; Watanabe, M. High Performance Dye-Sensitized Solar Cells Using Ionic Liquids as Their Electrolytes. *J. Photochem. Photobiol. A Chem.* **2004**, *164* (1–3), 87–92. https://doi.org/10.1016/j.jphotochem.2003.12.019.

(12) Armel, V.; Pringle, J. M.; Forsyth, M.; MacFarlane, D. R.; Officer, D. L.; Wagner, P. Ionic Liquid Electrolyte Porphyrin Dye Sensitised Solar Cells. *Chem. Commun.* **2010**, *46* (18), 3146. https://doi.org/10.1039/b926087k.

(13) Tedla, A.; Tai, Y. Influence of Binary Solvent System on the Stability and Efficiency of Liquid Dye Sensitized Solar Cells. *J. Photochem. Photobiol. A Chem.* **2018**, *358*, 70–75. https://doi.org/10.1016/j.jphotochem.2018.03.005.

(14) Widegren, J. A.; Magee, J. W. Density, Viscosity, Speed of Sound, and Electrolytic Conductivity for the Ionic Liquid 1-Hexyl-3-Methylimidazolium Bis(Trifluoromethylsulfonyl)Imide and Its Mixtures with Water †. *J. Chem. Eng. Data* **2007**, *52* (6), 2331–2338. https://doi.org/10.1021/je700329a.

(15) Wang, J.; Tian, Y.; Zhao, Y.; Zhuo, K. A Volumetric and Viscosity Study for the Mixtures of 1-n-Butyl-3-Methylimidazolium Tetrafluoroborate Ionic Liquid with Acetonitrile, Dichloromethane, 2-Butanone and N, N ? Dimethylformamide. *Green*

Chem. **2003**, *5* (5), 618. https://doi.org/10.1039/b303735e.
(16) Stoppa, A.; Hunger, J.; Buchner, R. Conductivities of Binary Mixtures of Ionic Liquids with Polar Solvents. *J. Chem. Eng. Data* **2009**, *54* (2), 472–479. https://doi.org/10.1021/je800468h.
(17) Stoppa, A.; Hunger, J.; Hefter, G.; Buchner, R. Structure and Dynamics of 1- N -Alkyl-3- N -Methylimidazolium Tetrafluoroborate + Acetonitrile Mixtures. *J. Phys. Chem. B* **2012**, *116* (25), 7509–7521. https://doi.org/10.1021/jp3020673.
(18) Wakai, C.; Oleinikova, A.; Weingärtner, H. Reply to "Comment On 'How Polar Are Ionic Liquids? Determination of the Static Dielectric Constant of an Imidazolium-Based Ionic Liquid by Microwave Spectroscopy'''''." *J. Phys. Chem. B* **2006**, *110* (11), 5824–5824. https://doi.org/10.1021/jp0601973.
(19) Znamenskiy, V.; Kobrak, M. N. Molecular Dynamics Study of Polarity in Room-Temperature Ionic Liquids. *J. Phys. Chem. B* **2004**, *108* (3), 1072–1079. https://doi.org/10.1021/jp035891m.
(20) Hagfeldt, A.; Boschloo, G.; Sun, L.; Kloo, L.; Pettersson, H. Dye-Sensitized Solar Cells. *Chem. Rev.* **2010**, *110* (11), 6595–6663. https://doi.org/10.1021/cr900356p.
(21) Kim, J. Y.; Kim, Y. H.; Kim, Y. S. Indoline Dyes with Various Acceptors for Dye-Sensitized Solar Cells. *Curr. Appl. Phys.* **2011**, *11* (1), S117–S121. https://doi.org/10.1016/j.cap.2010.11.098.
(22) Kim, S.; Lee, J. K.; Kang, S. O.; Ko, J.; Yum, J.-H.; Fantacci, S.; De Angelis, F.; Di Censo, D.; Nazeeruddin, M. K.; Grätzel, M. Molecular Engineering of Organic Sensitizers for Solar Cell Applications. *J. Am. Chem. Soc.* **2006**, *128* (51), 16701–16707. https://doi.org/10.1021/ja066376f.
(23) Listorti, A.; O'Regan, B.; Durrant, J. R. Electron Transfer Dynamics in Dye-Sensitized Solar Cells. *Chem. Mater.* **2011**, *23* (15), 3381–3399. https://doi.org/10.1021/cm200651e.
(24) Oum, K.; Lohse, P. W.; Flender, O.; Klein, J. R.; Scholz, M.; Lenzer, T.; Du, J.; Oekermann, T. Ultrafast Dynamics of the Indoline Dye D149 on Electrodeposited ZnO and Sintered ZrO2 and TiO2 Thin Films. *Phys. Chem. Chem. Phys.* **2012**, *14* (44), 15429. https://doi.org/10.1039/c2cp42961f.
(25) Shalini, S.; Balasundaraprabhu, R.; Kumar, T. S.; Prabavathy, N.; Senthilarasu, S.; Prasanna, S. Status and Outlook of Sensitizers/Dyes Used in Dye Sensitized Solar Cells (DSSC): A Review. *Int. J. Energy Res.* **2016**, *40* (10), 1303–1320. https://doi.org/10.1002/er.3538.
(26) Tang, Z.-M.; Lei, T.; Jiang, K.-J.; Song, Y.-L.; Pei, J. Benzothiadiazole Containing D-π-A Conjugated Compounds for Dye-Sensitized Solar Cells: Synthesis, Properties, and Photovoltaic Performances. *Chem. - An Asian J.* **2010**, *5* (8), 1911–1917. https://doi.org/10.1002/asia.201000158.
(27) Piątkowski, P.; Ratajska-Gadomska, B.; Gadomski, W. Probing Slow Dynamics by Ultrafast Process: Sol–Gel Transition Detected by Transient Absorption Spectroscopy of Quantum Dots. *J. Mol. Liq.* **2012**, *176* (39), 106–111. https://doi.org/10.1016/j.molliq.2012.06.027.
(28) Boschloo, G.; Hagfeldt, A. Characteristics of the Iodide/Triiodide Redox Mediator in Dye-Sensitized Solar Cells. *Acc. Chem. Res.* **2009**, *42* (11), 1819–1826. https://doi.org/10.1021/ar900138m.
(29) Hagfeldt, A.; Boschloo, G.; Sun, L.; Kloo, L.; Pettersson, H. Dye-Sensitized Solar Cells. *Chem. Rev.* **2010**, *110* (11), 6595–6663. https://doi.org/10.1021/cr900356p.
(30) Lohse, P. W.; Kuhnt, J.; Druzhinin, S. I.; Scholz, M.; Ekimova, M.; Oekermann, T.; Lenzer, T.; Oum, K. Ultrafast Photoinduced Relaxation Dynamics of the Indoline Dye D149 in Organic Solvents. *Phys. Chem. Chem. Phys.* **2011**, *13* (43), 19632.

https://doi.org/10.1039/c1cp22429h.
(31) Lin, Y. D.; Chow, T. J. Geometrical Effect of Stilbene on the Performance of Organic Dye-Sensitized Solar Cells. *J. Mater. Chem.* **2011**, *21* (38), 14907–14916. https://doi.org/10.1039/c1jm11623a.
(32) Fakis, M.; Stathatos, E.; Tsigaridas, G.; Giannetas, V.; Persephonis, P. Femtosecond Decay and Electron Transfer Dynamics of the Organic Sensitizer D149 and Photovoltaic Performance in Quasi-Solid-State Dye-Sensitized Solar Cells. *J. Phys. Chem. C* **2011**, *115* (27), 13429–13437. https://doi.org/10.1021/jp201143n.
(33) El-Zohry, A.; Orthaber, A.; Zietz, B. Isomerization and Aggregation of the Solar Cell Dye D149. *J. Phys. Chem. C* **2012**, *116* (50), 26144–26153. https://doi.org/10.1021/jp306636w.
(34) El-Zohry, A. M.; Roca-Sanjuán, D.; Zietz, B. Ultrafast Twisting of the Indoline Donor Unit Utilized in Solar Cell Dyes: Experimental and Theoretical Studies. *J. Phys. Chem. C* **2015**, *119* (5), 2249–2259. https://doi.org/10.1021/jp505649s.
(35) El-Zohry, A. M.; Zietz, B. Concentration and Solvent Effects on the Excited State Dynamics of the Solar Cell Dye D149: The Special Role of Protons. *J. Phys. Chem. C* **2013**, *117* (13), 6544–6553. https://doi.org/10.1021/jp400782g.
(36) Samanta, A. Solvation Dynamics in Ionic Liquids: What We Have Learned from the Dynamic Fluorescence Stokes Shift Studies. *J. Phys. Chem. Lett.* **2010**, *1* (10), 1557–1562. https://doi.org/10.1021/jz100273b.
(37) Samanta, A. Dynamic Stokes Shift and Excitation Wavelength Dependent Fluorescence of Dipolar Molecules in Room Temperature Ionic Liquids. *J. Phys. Chem. B* **2006**, *110* (28), 13704–13716. https://doi.org/10.1021/jp060441q.
(38) Sahu, P. K.; Das, S. K.; Sarkar, M. Fluorescence Response of a Dipolar Organic Solute in a Dicationic Ionic Liquid (IL): Is the Behavior of Dicationic IL Different from That of Usual Monocationic IL? *Phys. Chem. Chem. Phys.* **2014**, *16* (25), 12918–12928. https://doi.org/10.1039/C4CP01053A.
(39) Paul, A.; Samanta, A. Solute Rotation and Solvation Dynamics in an Alcohol-Functionalized Room Temperature Ionic Liquid †. *J. Phys. Chem. B* **2007**, *111* (18), 4724–4731. https://doi.org/10.1021/jp065790z.
(40) Paul, A.; Samanta, A. Effect of Nonpolar Solvents on the Solute Rotation and Solvation Dynamics in an Imidazolium Ionic Liquid. *J. Phys. Chem. B* **2008**, *112* (3), 947–953. https://doi.org/10.1021/jp077536s.
(41) Liang, M.; Zhang, X.-X.; Kaintz, A.; Ernsting, N. P.; Maroncelli, M. Solvation Dynamics in a Prototypical Ionic Liquid + Dipolar Aprotic Liquid Mixture: 1-Butyl-3-Methylimidazolium Tetrafluoroborate + Acetonitrile. *J. Phys. Chem. B* **2014**, *118* (5), 1340–1352. https://doi.org/10.1021/jp412086t.
(42) Karmakar, R.; Samanta, A. Steady-State and Time-Resolved Fluorescence Behavior of C153 and PRODAN in Room-Temperature Ionic Liquids. *J. Phys. Chem. A* **2002**, *106* (28), 6670–6675. https://doi.org/10.1021/jp0143591.
(43) Horng, M. L.; Gardecki, J. A.; Papazyan, A.; Maroncelli, M. Subpicosecond Measurements of Polar Solvation Dynamics: Coumarin 153 Revisited. *J. Phys. Chem.* **1995**, *99* (48), 17311–17337. https://doi.org/10.1021/j100048a004.
(44) Smortsova, Y.; Miannay, F.-A.; Oher, H.; Marekha, B.; Dubois, J.; Sliwa, M.; Kalugin, O.; Idrissi, A. Solvation Dynamics and Rotation of Coumarin 153 in a New Ionic Liquid/Molecular Solvent Mixture Model: [BMIM][TFSI]/Propylene Carbonate. *J. Mol. Liq.* **2017**, *226*, 48–55. https://doi.org/10.1016/j.molliq.2016.10.008.
(45) Smortsova, Y.; Miannay, F.-A.; Koverga, V.; Dubois, J.; Kalugin, O.; Idrissi, A. Fluorescent Probe Dependence of the Solvation Dynamics in Ionic Liquid BmimBF4 and Propylene Carbonate Mixtures: A Time-Resolved Fluorescence and Quantum

Chemistry Study. *J. Mol. Liq.* **2019**, *282*, 39–50. https://doi.org/10.1016/j.molliq.2019.02.123.
(46) Sarkar, S.; Mandal, S.; Ghatak, C.; Rao, V. G.; Ghosh, S.; Sarkar, N. Photoinduced Electron Transfer in an Imidazolium Ionic Liquid and in Its Binary Mixtures with Water, Methanol, and 2-Propanol: Appearance of Marcus-Type of Inversion. *J. Phys. Chem. B* **2012**, *116* (4), 1335–1344. https://doi.org/10.1021/jp2075995.
(47) Nandi, S.; Parui, S.; Jana, B.; Bhattacharyya, K. Local Environment of Organic Dyes in an Ionic Liquid-Water Mixture: FCS and MD Simulation. *J. Chem. Phys.* **2018**, *149* (5). https://doi.org/10.1063/1.5027458.
(48) Mandal, S.; Ghosh, S.; Banerjee, C.; Kuchlyan, J.; Sarkar, N. Roles of Viscosity, Polarity, and Hydrogen-Bonding Ability of a Pyrrolidinium Ionic Liquid and Its Binary Mixtures in the Photophysics and Rotational Dynamics of the Potent Excited-State Intramolecular Proton-Transfer Probe 2,2′-Bipyridine-3,3′-Diol. *J. Phys. Chem. B* **2013**, *117* (22), 6789–6800. https://doi.org/10.1021/jp4025443.
(49) Lohse, P. W.; Bartels, N.; Stoppa, A.; Buchner, R.; Lenzer, T.; Oum, K. Dielectric Relaxation and Ultrafast Transient Absorption Spectroscopy of [C6mim]+[Tf2N]−/Acetonitrile Mixtures. *Phys. Chem. Chem. Phys.* **2012**, *14* (10), 3596. https://doi.org/10.1039/c2cp23704k.
(50) Chowdhury, P. K.; Halder, M.; Sanders, L.; Calhoun, T.; Anderson, J. L.; Armstrong, D. W.; Song, X.; Petrich, J. W. Dynamic Solvation in Room-Temperature Ionic Liquids †. *J. Phys. Chem. B* **2004**, *108* (29), 10245–10255. https://doi.org/10.1021/jp0376828.
(51) Fakis, M.; Hrobárik, P.; Stathatos, E.; Giannetas, V.; Persephonis, P. A Time Resolved Fluorescence and Quantum Chemical Study of the Solar Cell Sensitizer D149. *Dye. Pigment.* **2013**, *96* (1), 304–312. https://doi.org/10.1016/j.dyepig.2012.07.025.
(52) Piątkowski, P.; Ratajska-Gadomska, B.; Gadomski, W. Probing Slow Dynamics by Ultrafast Process: Sol–Gel Transition Detected by Transient Absorption Spectroscopy of Quantum Dots. *J. Mol. Liq.* **2012**, *176*, 106–111. https://doi.org/10.1016/j.molliq.2012.06.027.
(53) Le Bahers, T.; Pauporté, T.; Scalmani, G.; Adamo, C.; Ciofini, I. A TD-DFT Investigation of Ground and Excited State Properties in Indoline Dyes Used for Dye-Sensitized Solar Cells. *Phys. Chem. Chem. Phys.* **2009**, *11* (47), 11276. https://doi.org/10.1039/b914626a.
(54) Chen, Z.; Lee, C.; Lenzer, T.; Oum, K. Solvent Effects on the S0(11Ag-) → S2(11Bu+) Transition of β-Carotene, Echinenone, Canthaxanthin, and Astaxanthin in Supercritical CO2 and CF3H. *J. Phys. Chem. A* **2006**, *110* (39), 11291–11297. https://doi.org/10.1021/jp0643247.
(55) Lohse, P. W.; Bürsing, R.; Lenzer, T.; Oum, K. Exploring 12′-Apo-β-Carotenoic-12′-Acid as an Ultrafast Polarity Probe for Ionic Liquids. *J. Phys. Chem. B* **2008**, *112* (10), 3048–3057. https://doi.org/10.1021/jp710766z.
(56) Golibrzuch, K.; Ehlers, F.; Scholz, M.; Oswald, R.; Lenzer, T.; Oum, K.; Kim, H.; Koo, S. Ultrafast Excited State Dynamics and Spectroscopy of 13,13′-Diphenyl- β-Carotene. *Phys. Chem. Chem. Phys.* **2011**, *13* (13), 6340–6351. https://doi.org/10.1039/c0cp02525a.
(57) Zhu, G.; Zhang, L.; Wang, Y.; Xu, X.; Peng, X. Interactions between Pyrene and Pyridinium Ionic Liquids Studied by Ultraviolet–Visible Spectroscopy. *J. Mol. Liq.* **2016**, *213*, 289–293. https://doi.org/10.1016/j.molliq.2015.11.026.
(58) Reichardt, C. Solvatochromic Dyes as Solvent Polarity Indicators. *Chem. Rev.* **1994**, *94* (8), 2319–2358. https://doi.org/10.1021/cr00032a005.
(59) Poole, C. F. Chromatographic and Spectroscopic Methods for the Determination of

Solvent Properties of Room Temperature Ionic Liquids. *J. Chromatogr. A* **2004**, *1037* (1–2), 49–82. https://doi.org/10.1016/j.chroma.2003.10.127.
(60) Lee, J.-M.; Ruckes, S.; Prausnitz, J. M. Solvent Polarities and Kamlet−Taft Parameters for Ionic Liquids Containing a Pyridinium Cation. *J. Phys. Chem. B* **2008**, *112* (5), 1473–1476. https://doi.org/10.1021/jp076895k.
(61) Mancini, P. M.; Fortunato, G. G.; Adam, C. G.; Vottero, L. R. Solvent Effects on Chemical Processes: New Solvents Designed on the Basis of the Molecular–Microscopic Properties of (Molecular Solvent + 1,3-Dialkylimidazolium) Binary Mixtures. *J. Phys. Org. Chem.* **2008**, *21* (2), 87–95. https://doi.org/10.1002/poc.1227.
(62) van Wilderen, L. J. G. W.; Lincoln, C. N.; van Thor, J. J. Modelling Multi-Pulse Population Dynamics from Ultrafast Spectroscopy. *PLoS One* **2011**, *6* (3), e17373. https://doi.org/10.1371/journal.pone.0017373.
(63) Sobuś, J.; Karolczak, J.; Komar, D.; Anta, J. A.; Ziółek, M. Transient States and the Role of Excited State Self-Quenching of Indoline Dyes in Complete Dye-Sensitized Solar Cells. *Dye. Pigment.* **2015**, *113*, 692–701. https://doi.org/10.1016/j.dyepig.2014.10.008.
(64) Koverga, V. A.; Smortsova, Y.; Miannay, F. A.; Kalugin, O. N.; Takamuku, T.; Jedlovszky, P.; Marekha, B.; Cordeiro, M. N. D. S.; Idrissi, A. Distance Angle Descriptors of the Interionic and Ion–Solvent Interactions in Imidazolium-Based Ionic Liquid Mixtures with Aprotic Solvents: A Molecular Dynamics Simulation Study. *J. Phys. Chem. B* **2019**, *123* (28), 6065–6075. https://doi.org/10.1021/acs.jpcb.9b03838.
(65) Polok, K.; Beisert, M.; Świątek, A.; Maity, N.; Piatkowski, P.; Gadomski, W.; Miannay, F. A.; Idrissi, A. Dynamics in the BMIM PF 6 /Acetonitrile Mixtures Observed by Femtosecond Optical Kerr Effect and Molecular Dynamics Simulations. *Phys. Chem. Chem. Phys.* **2020**, *22* (42), 24544–24554. https://doi.org/10.1039/D0CP03847D.
(66) Ravi Kumar, V.; Verma, C.; Umapathy, S. Molecular Dynamics and Simulations Study on the Vibrational and Electronic Solvatochromism of Benzophenone. *J. Chem. Phys.* **2016**, *144* (6), 064302. https://doi.org/10.1063/1.4941058.
(67) Kwac, K.; Geva, E. Solvation Dynamics of Formylperylene Dissolved in Methanol-Acetonitrile Liquid Mixtures: A Molecular Dynamics Study. *J. Phys. Chem. B* **2013**, *117* (34), 9996–10006. https://doi.org/10.1021/jp405818f.
(68) Blazhynska, M. M.; Stepaniuk, D. S.; Koverga, V.; Kyrychenko, A.; Idrissi, A.; Kalugin, O. N. Structure and Dynamics of TiO2-Anchored D205 Dye in Ionic Liquids and Acetonitrile. *J. Mol. Liq.* **2021**, *332*, 115811. https://doi.org/10.1016/j.molliq.2021.115811.

Supporting Information:

Table S1: Different global analysis time constants of D149 in $BmimBF_4$-ACN mixtures.

X_{IL}	τ_1 (ps)	τ_2 (ps)	τ_3 (ps)	τ_4 (ps)
0	0.08 ± 0.003	0.65 ± 0.03	33.34 ± 2.14	275.65 ± 5.97
0.05	0.10 ± 0.04	0.81 ± 0.15	27.92 ± 1.21	234.91 ± 2.55
0.10	0.14 ± 0.04	0.90 ± 0.13	16.29 ± 0.68	210.72 ± 1.09
0.20	0.17 ± 0.07	1.04 ± 0.89	18.71 ± 1.56	248.61 ± 7.59
0.50	0.25 ± 0.06	2.65 ± 0.47	30.23 ± 4.71	450.02 ± 7.16
0.80	0.27 ± 0.09	5.68 ± 1.07	69.58 ± 8.59	706.73 ± 8.91
1	0.51 ± 0.04	10.39 ± 1.86	120.71 ± 10.35	912.43 ± 10.28

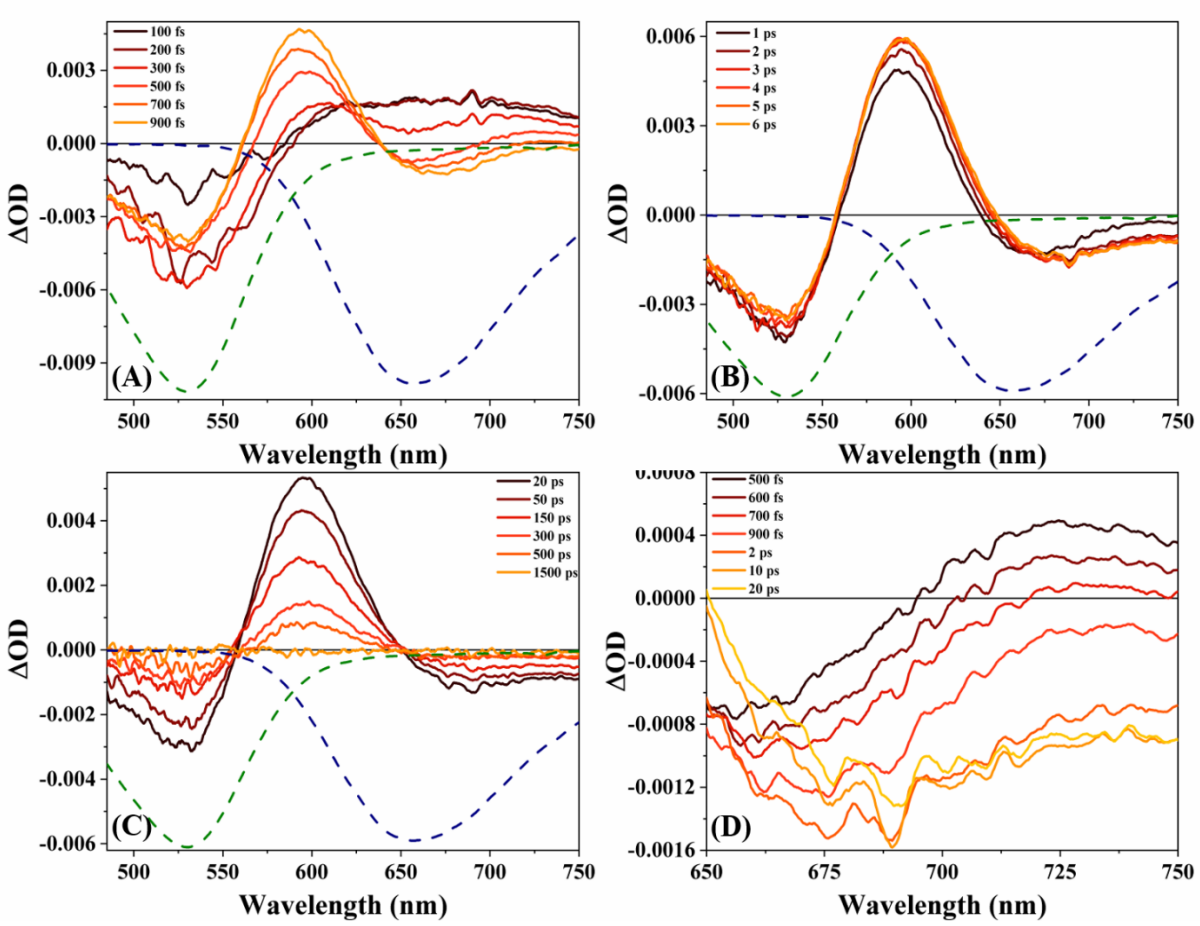

Figure S1: Transient Absorption spectra of D149 in ACN, (A) short timescale (100-900 fs), (B) middle timescale (1-6 ps), (C) long timescale (20-1500 ps), (D) solvation timescale. Dashed spectra are steady state absorption (green) and emission (blue) spectra.

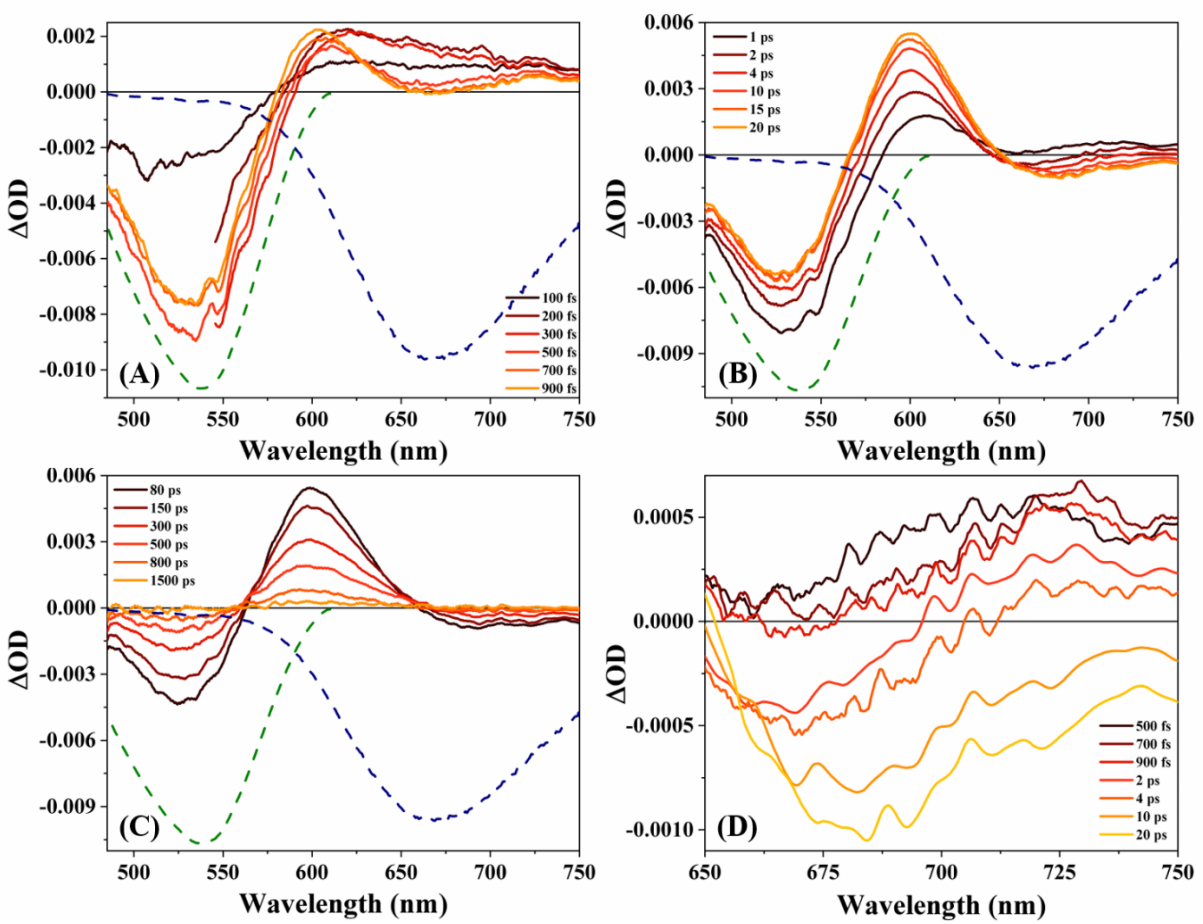

Figure S2: Transient Absorption spectra of D149 in $BmimBF_4$–ACN binary mixture (X_{IL}= 0.05), (A) short timescale (100-900 fs), (B) middle timescale (1-20 ps), (C) long timescale (80-1500 ps), (D) solvation timescale. Dashed spectra are steady state absorption (green) and emission (blue) spectra.

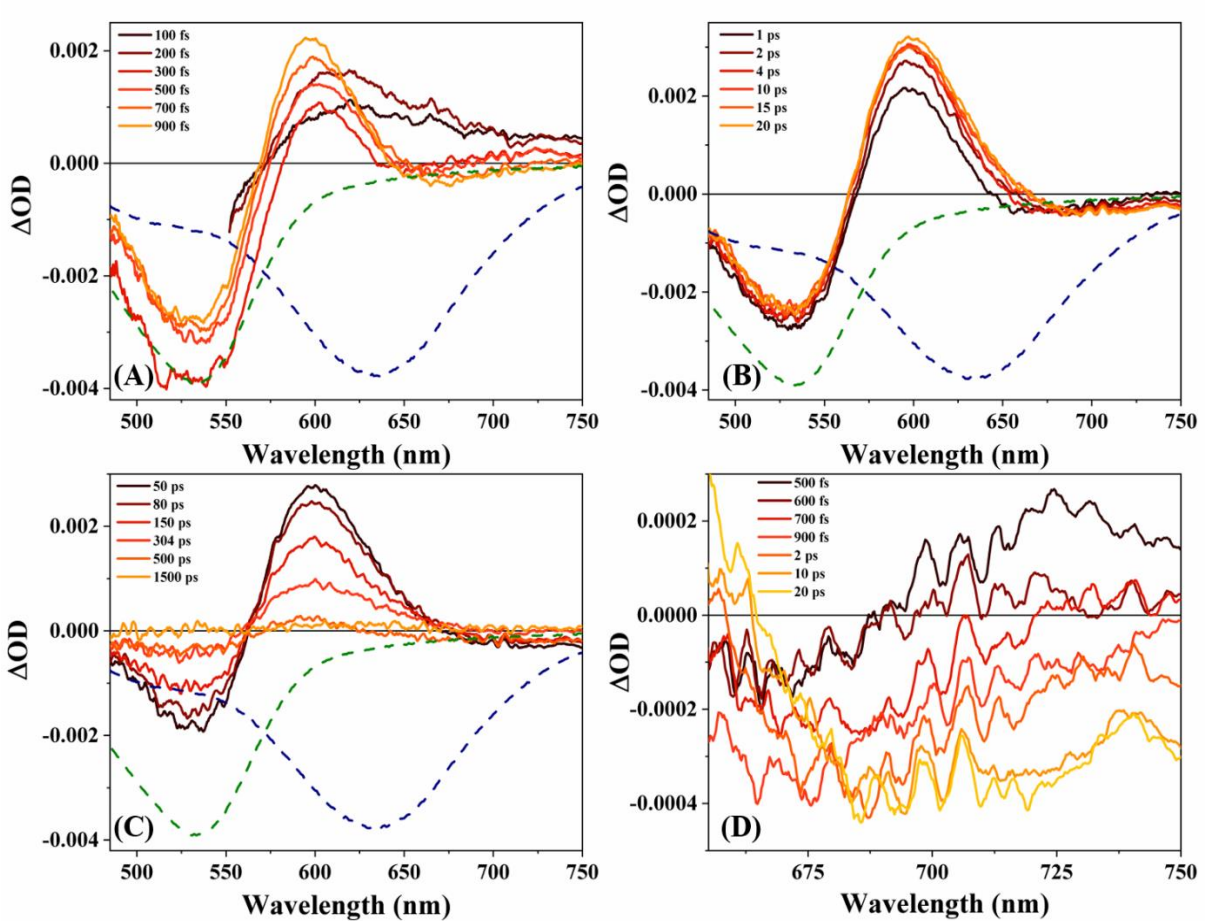

Figure S3: Transient Absorption spectra of D149 in $BmimBF_4$–ACN binary mixture (X_{IL}= 0.10), (A) short timescale (100-900 fs), (B) middle timescale (1-20 ps), (C) long timescale (50-1500 ps), (D) solvation timescale. Dashed spectra are steady state absorption (green) and emission (blue) spectra.

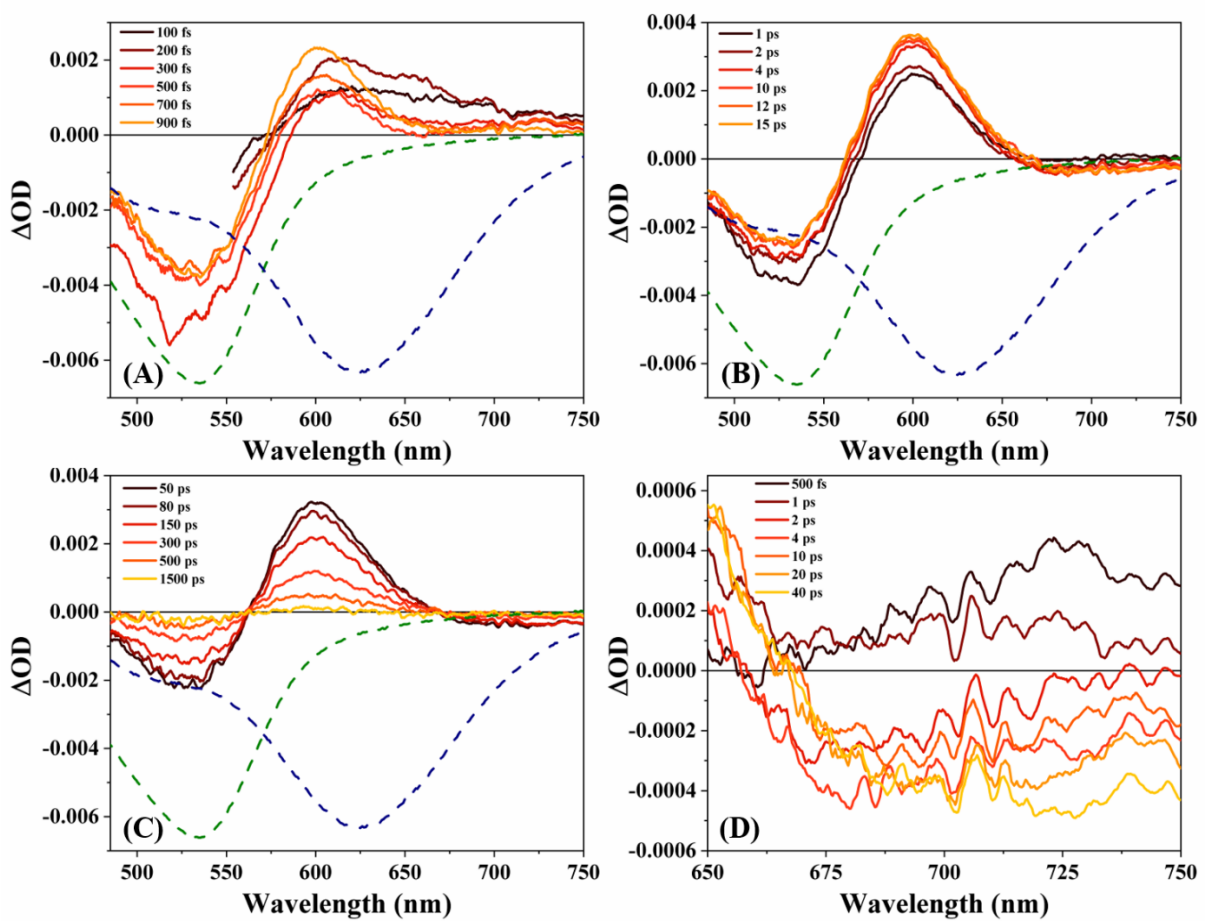

Figure S4: Transient Absorption spectra of D149 in $BmimBF_4$–ACN binary mixture (X_{IL}= 0.20), (A) short timescale (100-900 fs), (B) middle timescale (1-15 ps), (C) long timescale (50-1500 ps), (D) solvation timescale. Dashed spectra are steady state absorption (green) and emission (blue) spectra.

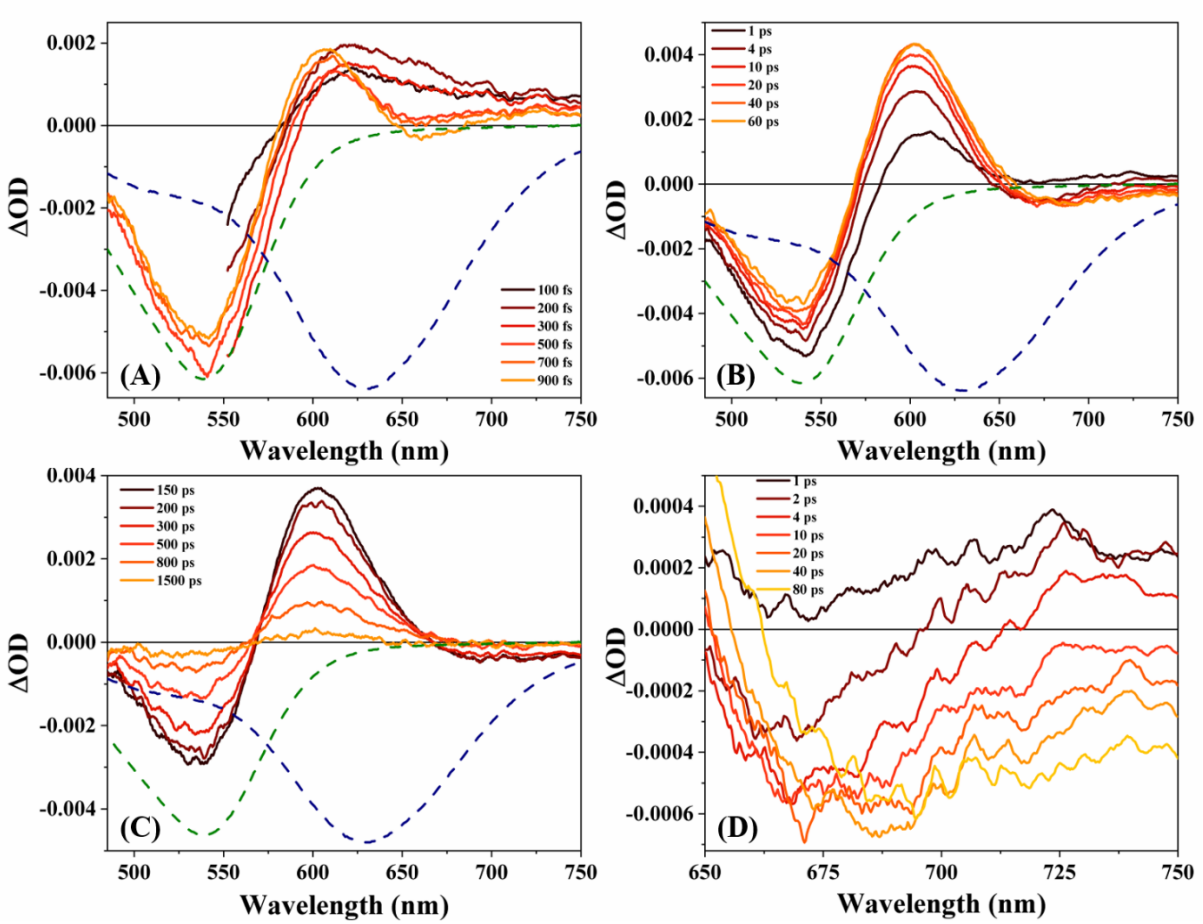

Figure S5: Transient Absorption spectra of D149 in $BmimBF_4$–ACN binary mixture (X_{IL}= 0.50), (A) short timescale (100-900 fs), (B) middle timescale (1-60 ps), (C) long timescale (150-1500 ps), (D) solvation timescale. Dashed spectra are steady state absorption (green) and emission (blue) spectra.

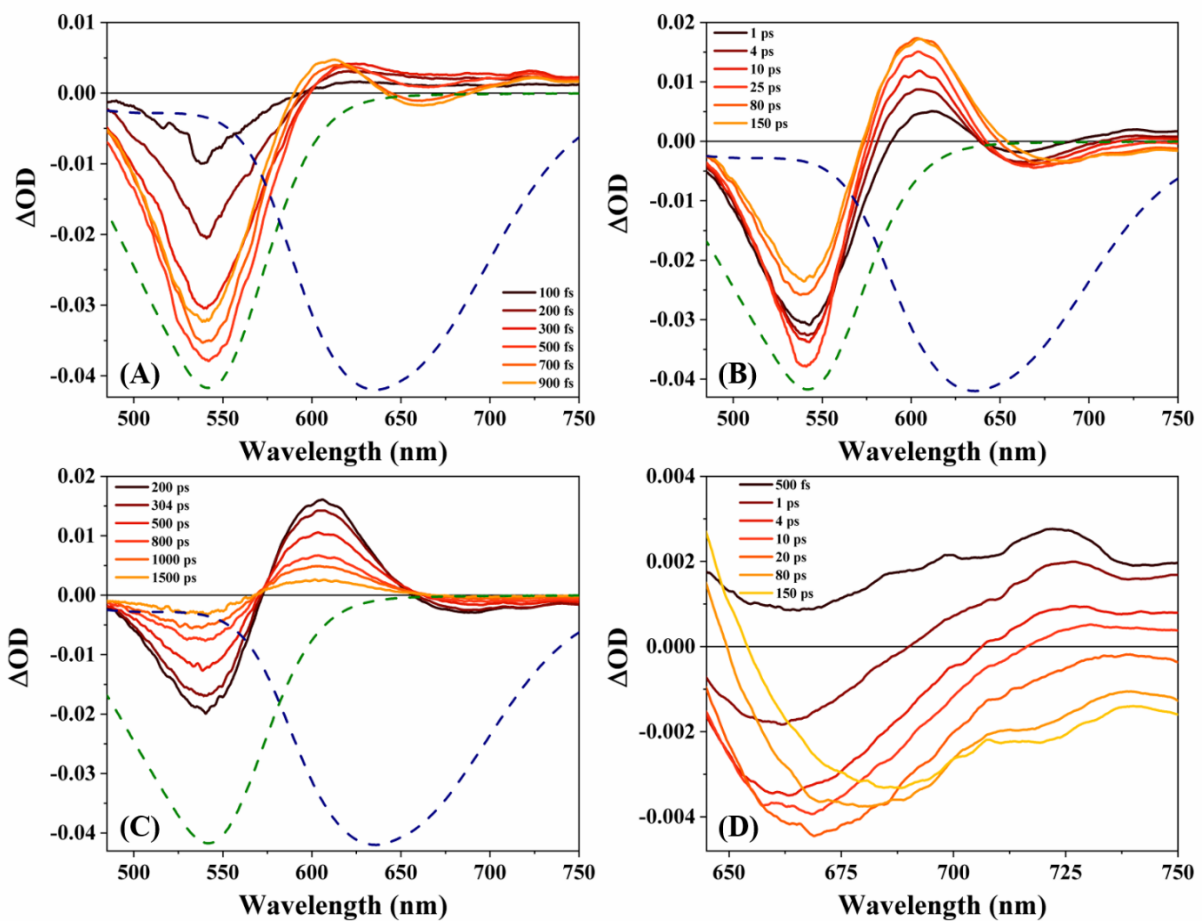

Figure S6: Transient Absorption spectra of D149 in $BmimBF_4$–ACN binary mixture (X_{IL}= 0.80), (A) short timescale (100-900 fs), (B) middle timescale (1-150 ps), (C) long timescale (200-1500 ps), (D) solvation timescale. Dashed spectra are steady state absorption (green) and emission (blue) spectra.

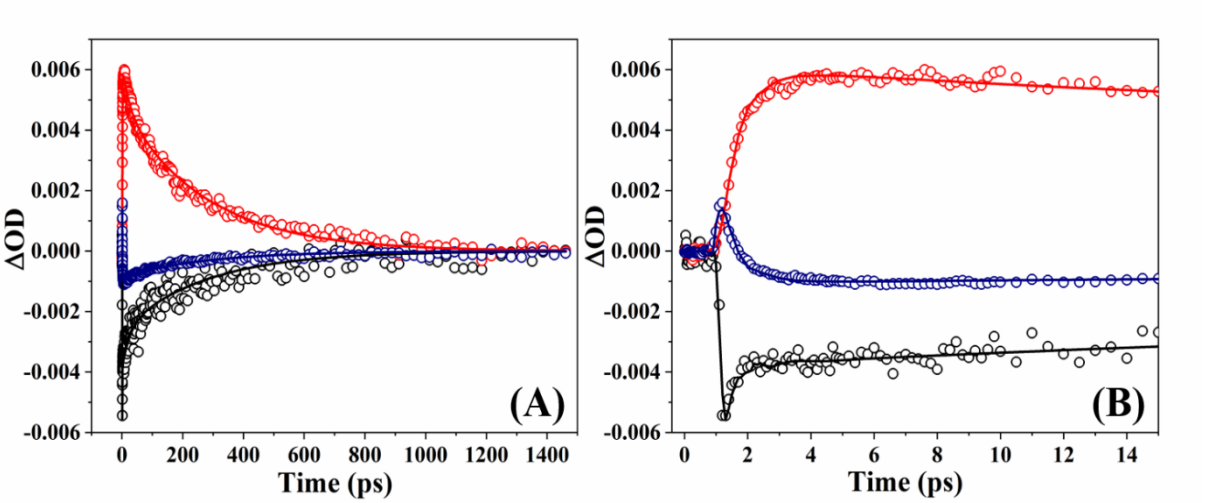

Figure S7: Experimental (hollow circles) and fitted (line) kinetic traces of D149 in ACN at different wavelengths 525 nm (black), 600 nm (red) and 720 nm (blue) of TA spectrum. (A) long timescale (0-1.5 ns), (B) short timescale (0-15 ps).

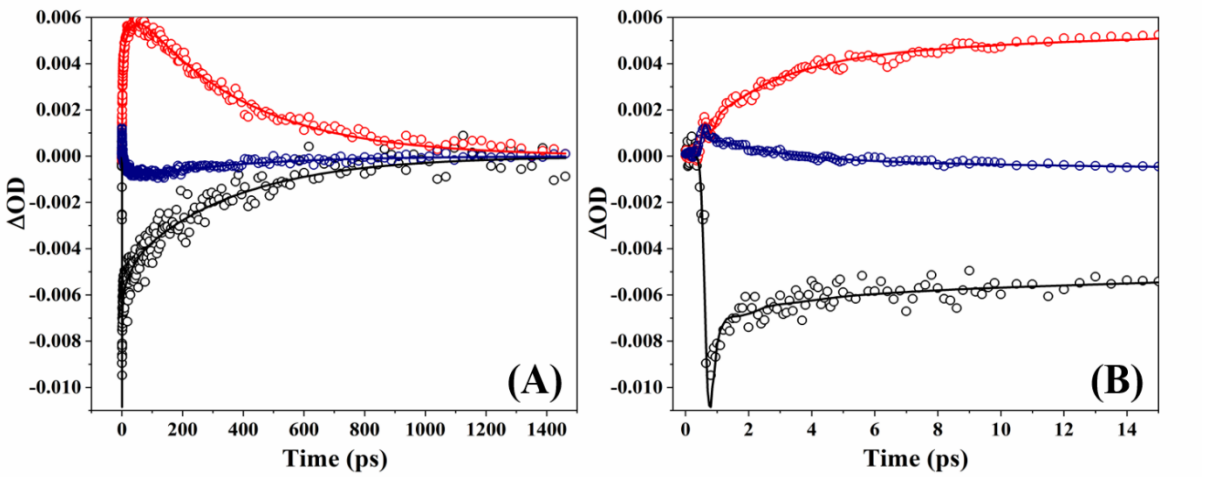

Figure S8: Experimental (hollow circles) and fitted (line) kinetic traces of D149 in $BmimBF_4$–ACN binary mixture (X_{IL}= 0.05) at different wavelengths 525 nm (black), 600 nm (red) and 720 nm (blue) of TA spectrum. (A) long timescale (0-1.5 ns), (B) short timescale (0-15 ps).

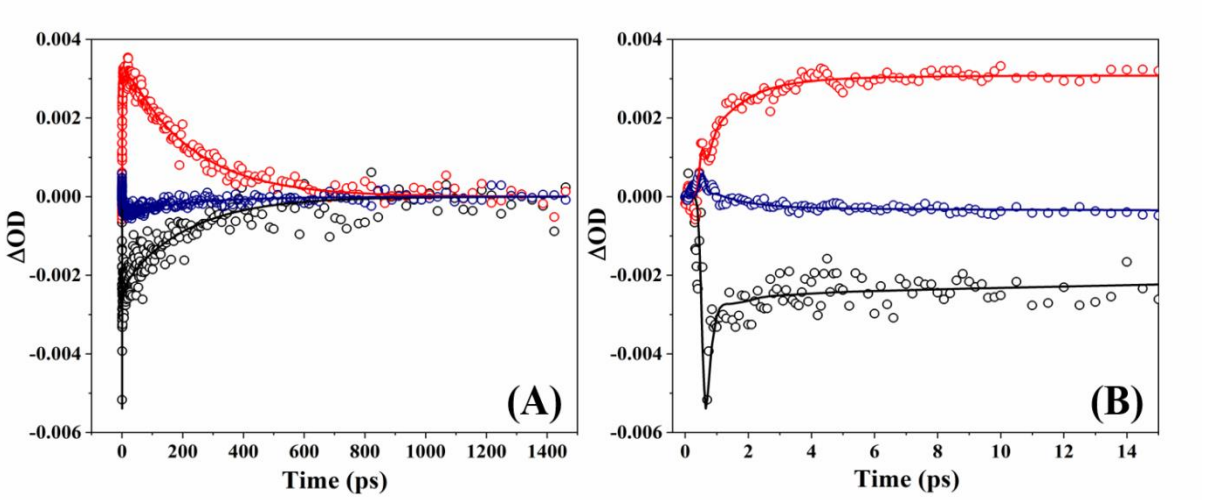

Figure S9: Experimental (hollow circles) and fitted (line) kinetic traces of D149 in $BmimBF_4$–ACN binary mixture (X_{IL}= 0.10) at different wavelengths 525 nm (black), 600 nm (red) and 720 nm (blue) of TA spectrum. (A) long timescale (0-1.5 ns), (B) short timescale (0-15 ps).

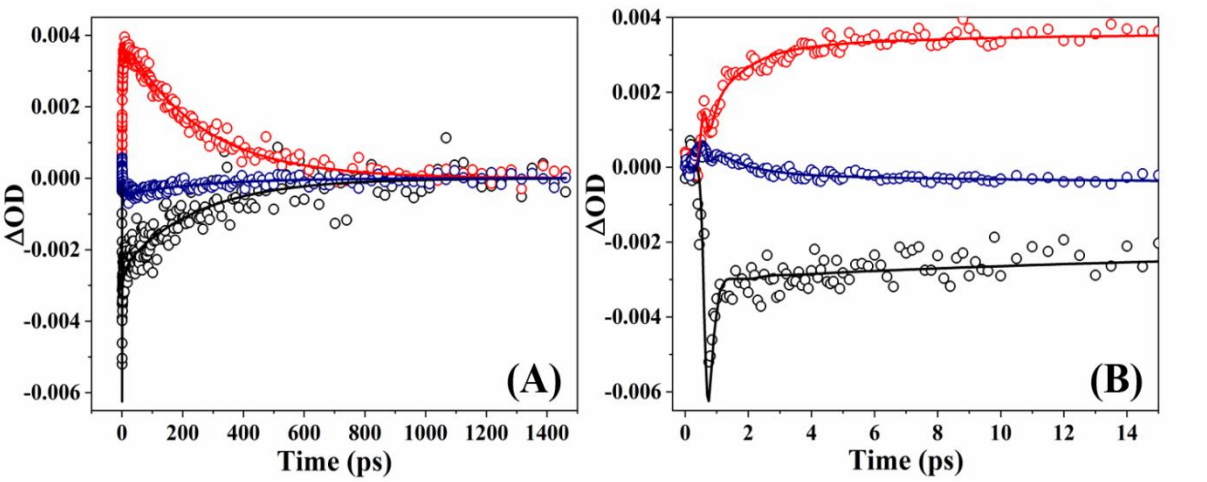

Figure S10: Experimental (hollow circles) and fitted (line) kinetic traces of D149 in $BmimBF_4$–ACN binary mixture (X_{IL}= 0.20) at different wavelengths 525 nm (black), 600 nm (red) and 720 nm (blue) of TA spectrum. (A) long timescale (0-1.5 ns), (B) short timescale (0-15 ps).

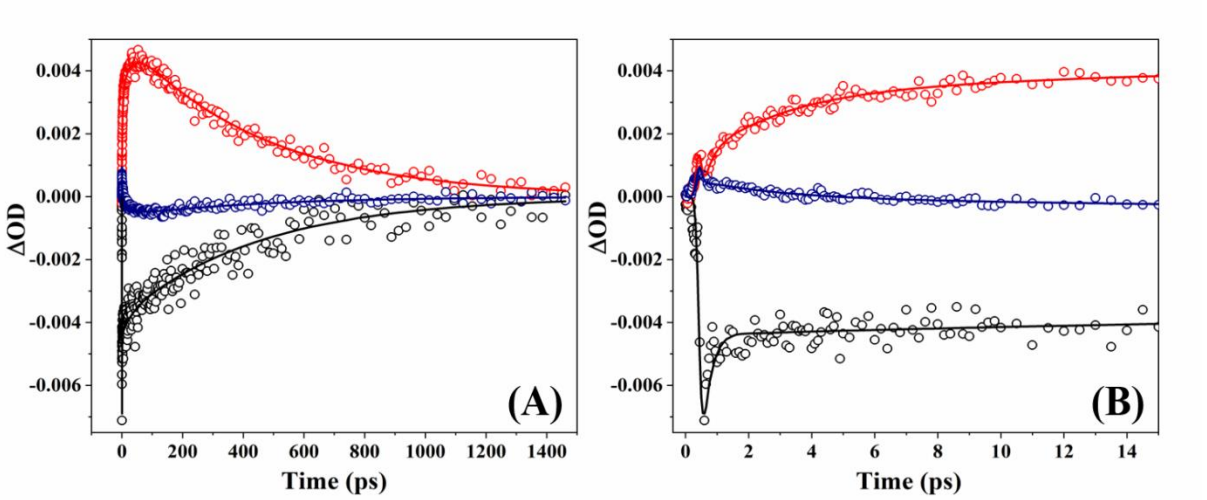

Figure S11: Experimental (hollow circles) and fitted (line) kinetic traces of D149 in $BmimBF_4$–ACN binary mixture (X_{IL}= 0.50) at different wavelengths 525 nm (black), 600 nm (red) and 720 nm (blue) of TA spectrum. (A) long timescale (0-1.5 ns), (B) short timescale (0-15 ps).

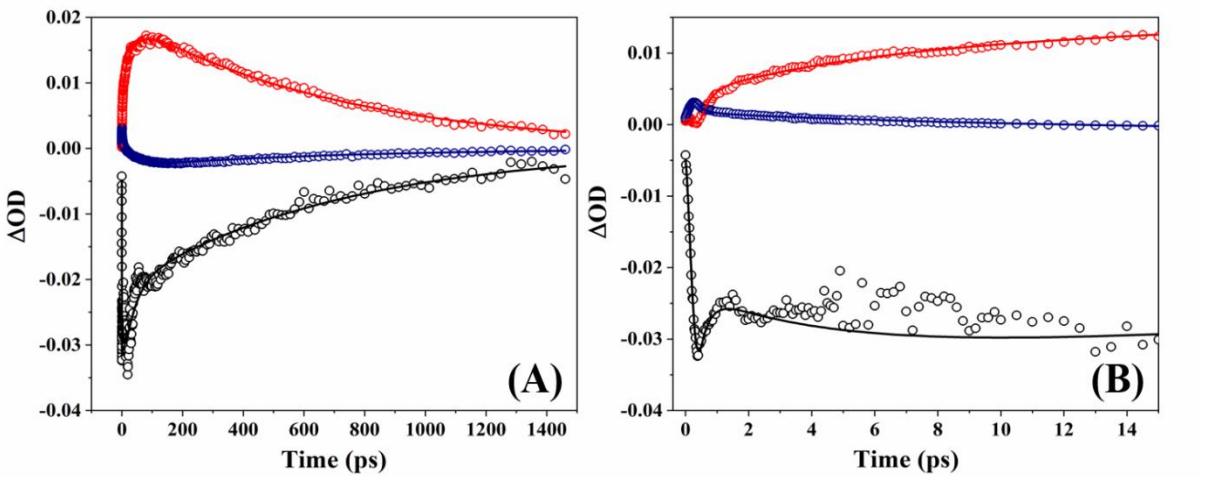

Figure S12: Experimental (hollow circles) and fitted (line) kinetic traces of D149 in $BmimBF_4$–ACN binary mixture (X_{IL}= 0.80) at different wavelengths 525 nm (black), 600 nm (red) and 720 nm (blue) of TA spectrum. (A) long timescale (0-1.5 ns), (B) short timescale (0-15 ps).

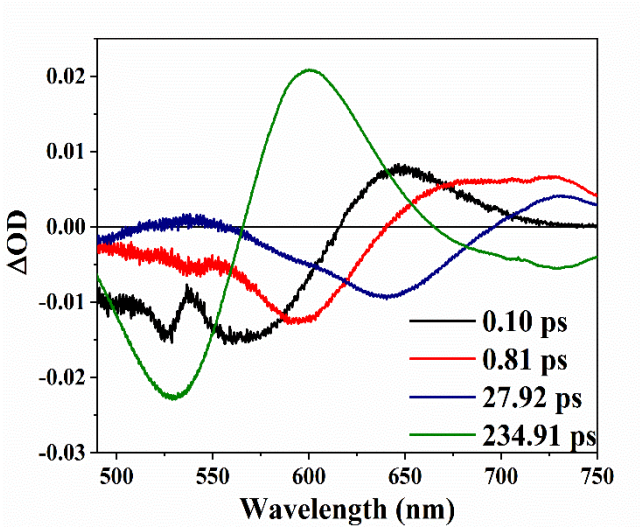

Figure S13: DAS of D149 in $BmimBF_4$-ACN binary mixture (X_{IL}= 0.05).

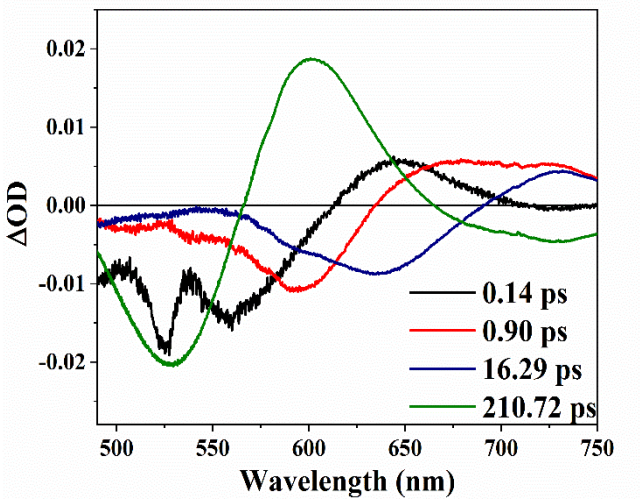

Figure S14: DAS of D149 in $BmimBF_4$-ACN binary mixture (X_{IL}= 0.10).

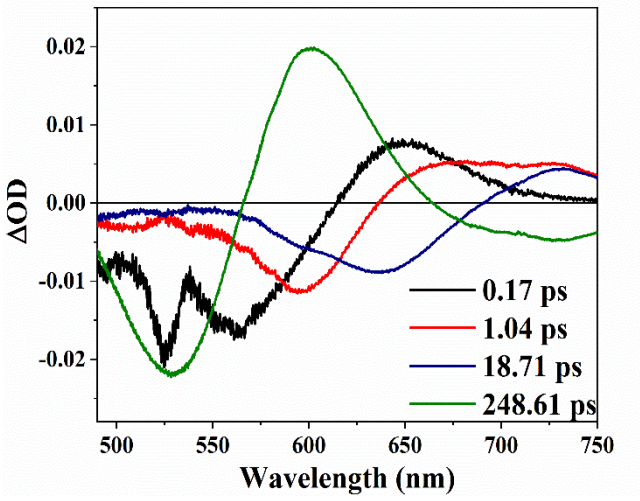

Figure S15: DAS of D149 in $BmimBF_4$-ACN binary mixture (X_{IL}= 0.20).

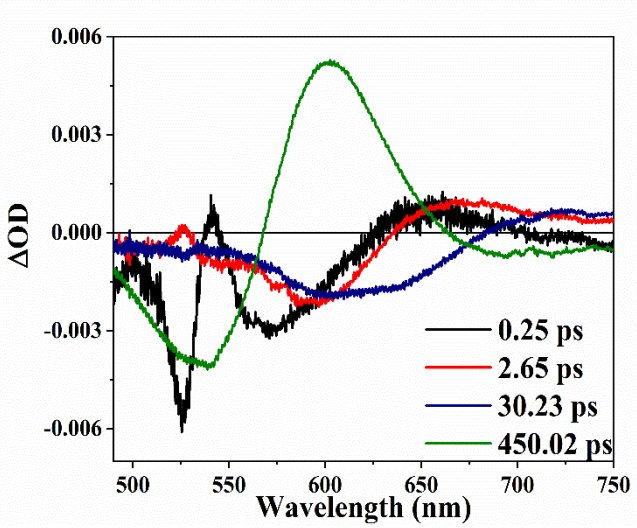

Figure S16: DAS of D149 in $BmimBF_4$-ACN binary mixture (X_{IL}= 0.50).

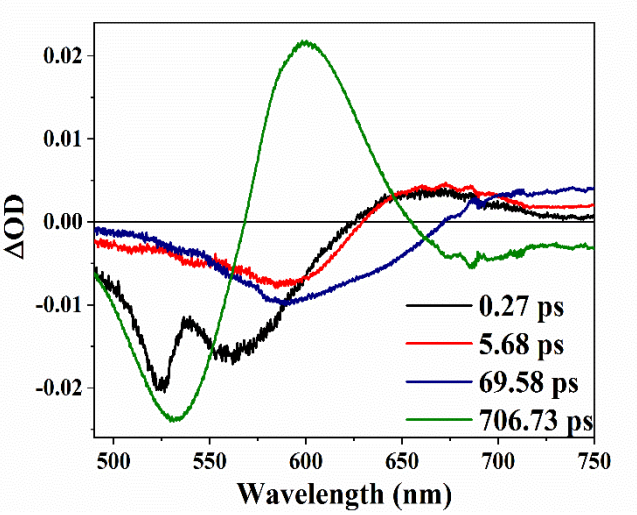

Figure S17: DAS of D149 in $BmimBF_4$-ACN binary mixture (X_{IL}= 0.80).